RDS RESEARCH AND DATA SYSTEMS, INC.

9420 ANNAPOLIS ROAD, LANHAM, MD. 20801 (301) 459-0001

A STUDY OF RADIO FREQUENCY INTERFERENCE WITH THE NIMBUS-7 SCANNING MULTICHANNEL MICROWAVE RADIOMETER (SMMR)

A STUDY OF RADIO FREQUENCY INTERFERENCE WITH THE NIMBUS-7 SCANNING MULTICHANNEL MICROWAVE RADIOMETER (SMMR)

Prepared For

NATIONAL AERONAUTICS AND SPACE ADMINISTRATION
GODDARD SPACE FLIGHT CENTER
GREENBELT, MARYLAND 20771

Under

CONTRACT NO.: NAS 5-25997

NOVEMBER 5, 1980

Prepared By

JOHN A. KOGUT

RESEARCH AND DATA SYSTEMS, INC.
9420 ANNAPOLIS ROAD
LANHAM, MARYLAND 20801

TABLE OF CONTENTS

SECTION

1.0 INTRODUCTION

2.0 RADIO FREQUENCY INTERFERENCE ANALYSIS AND RESULTS

3.0 CONCLUSIONS

4.0 REFERENCES

1.0 INTRODUCTION

One of the important objectives of the NIMBUS-7 Scanning Multichannel Microwave Radiometer (SMMR) is to demonstrate the feasibility of all weather measurements of various ocean parameters; such as sea surface temperature (SST) and near surface wind speed (WS). These ocean parameters can be determined from multispectral measurements of ocean brightness temperatures in the microwave region of the electromagnetic spectrum. These microwave measurements, however, are distorted if the field of view of the SMMR antenna encounters radio transmissions from terrestrial sources. This task was directed at identifying sources of terrestrial Radio Frequency Interference (RFI) in the SMMR ocean data and determining its extent and characteristics over different ocean areas on the earth. The SMMR instrument (Figure 1.0-1) provides orthogonally polarized antenna temperature measurements at five microwave frequencies; 6.6 GHz, 10.7 GHz, 18.0 GHz, 21.0 GHz, and 37.0 GHz. The instrument employs Dicke type radiometers at all frequencies. At the four lower frequencies alternate polarizations are measured during successive scans of the SMMR antenna, while at 37.0 GHz there is a radiometer operating continually at each polarization. The radiometers use an ambient RF termination, and a horn viewing deep space as a two point reference system. The main SMMR antenna is composed of a parabolic reflector illuminating a single feedhorn. The antennas main beam is offset 42°from nadir and scans the earth in a conical pattern with a half angle of about 25°(Figure 1.0-2).

The SMMR data processing can be divided into three major steps. In the first step the SMMR data, along with spacecraft orbit and attitude information, is extracted from the data telemetered from the spacecraft to the ground station and put onto magnetic tapes. In the second step, the SMMR antenna temperatures and geophysical parameters are computed from the sensor readings, put into various map formats and placed on tape. In the final step film products are produced from the mapped SMMR data.

For the analysis done here, SMMR data tapes containing earth located brightness temperatures from step 2 above were used with an algorithm to compute sea surface temperatures using the measured ocean brightness temperatures.

SMMR INSTRUMENT CONFIGURATION

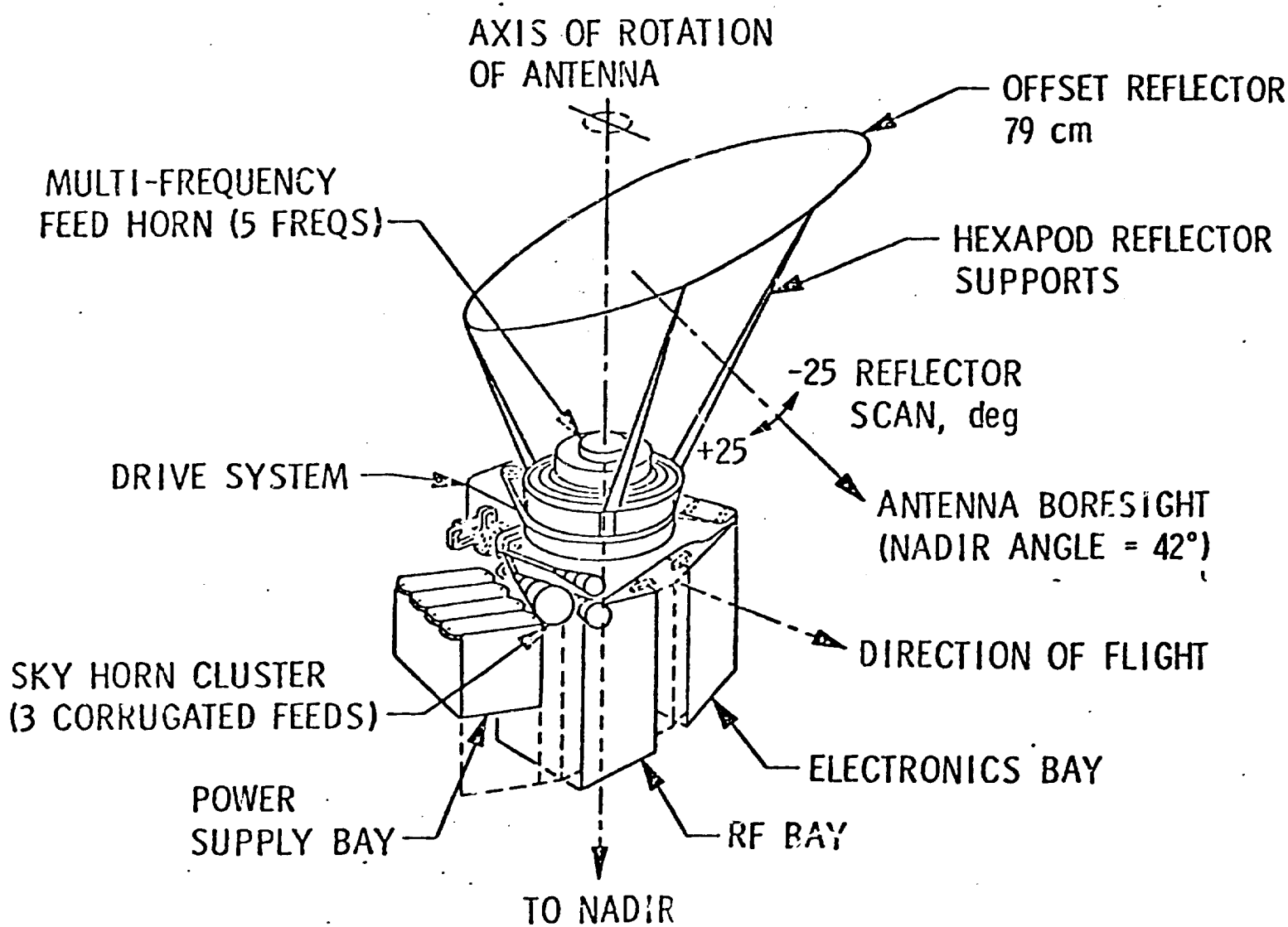

Figure 1.0-1

NIMBUS-G
SMMR SCAN GEOMETRY

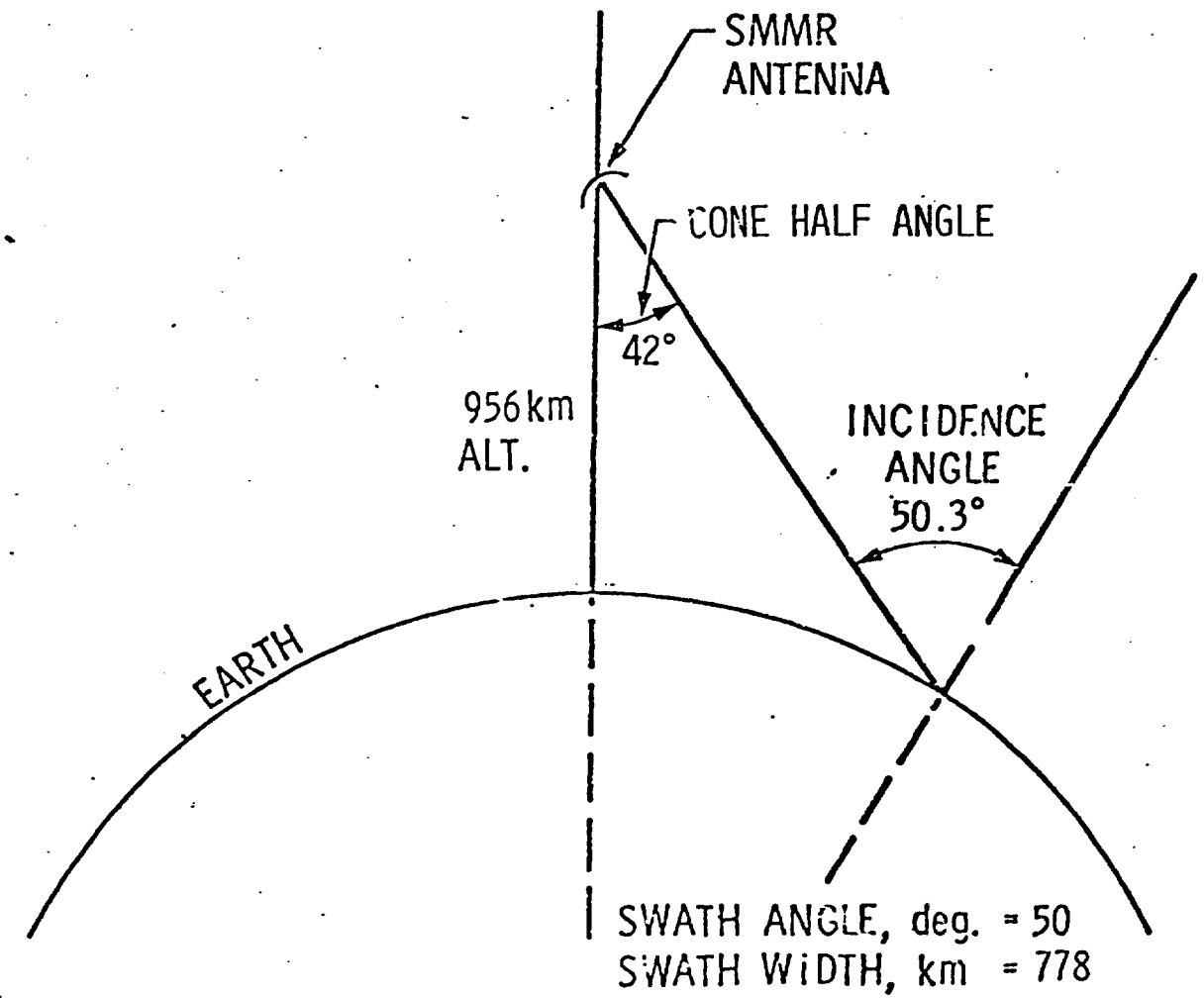

Figure 1.0-2

This analysis of SMMR radio frequency interference with ocean observations was divided into two parts. First, all the available SMMR brightness temperatures were examined to identify isolated intense point sources of RFI in the ocean data. Secondly the extent to which RFI significantly affects SMMR-derived sea surface temperatures over broad coastal regions was analyzed.

This study is performed under the assumption that

(1) the brightness temperatures are well calibrated and

(2) sidelobe corrections are properly implemented in these calibrated data.

2.0 RADIO FREQUENCY INTERFERENCE ANALYSIS AND RESULTS

Passive mirowave sensors such as the NIMBUS-7 SMMR may experience radio frequency interference arising from a number of terrestrial sources including microwave relay links, military, commercial, and research radars, and satellite telemetry links. Figure 2.0-1a (Friebaum 1975) illustrates the frequency sharing problems which may contribute to SMMR RFI. Figure 2.0-1b (Friebaum 1975) compares the space and terrestrial frequency allocations in the spectral range from 0.1 to 275 GHz with arrows indicating the five frequencies allocated to SMMR. It can be seen from this figure that with the exception of the 21.0 GHz channel, all the SMMR channels fall within bands allocated to terrestrial users. Based on these considerations it is reasonable to expect SMMR to experience radio frequency interference at various times during its operation.

The SMMR data used in this task was taken from the SMMR CELL-ALL tape, a product of the second stage of SMMR data processing. The CELL-ALL tape is a 9-track, 1600 BPI, no label tape containing one orbit of SMMR data per file. The logical record size is 15120 bytes and each logical record contains earth located SMMR brightness temperatures for a block 780 km by 780 km on the surface of the earth. The antenna temperature measurements from the SMMR are converted to brightness temperatures (T_b) and averaged into grids of various sizes based on the frequency of the observation.

The SMMR CELL-ALL tape observations are currently available for two time periods, October 25 to November 25, 1978, and February 15 to March 17, 1979. Table 2.0-I shows when good SMMR data is available within these two time periods. There is a total of 42 days worth of good SMMR data during these two time periods.

The SMMR brightness temperatures for each cell of the 780 km x 780 km block have been corrected for the effects of the antenna sidelobe pattern. In addition the CELL-ALL tape T_b's have been corrected for the effects of polarization mixing between the vertically and horizontally polarized components of the signal received by the SMMR antenna. New 6250 BPI CELL-ALL tapes having the same format as the 1600 BPI CELL-ALL tapes, but with the T_b's corrected for polarization mixing, and more days of data per tape, were produced for the October--November 1978 and February-March 1979 CELL-ALL data. These 6250 BPI tape

FIGURE 2.0-1a.

FREQUENCY SHARING PROBLEMS

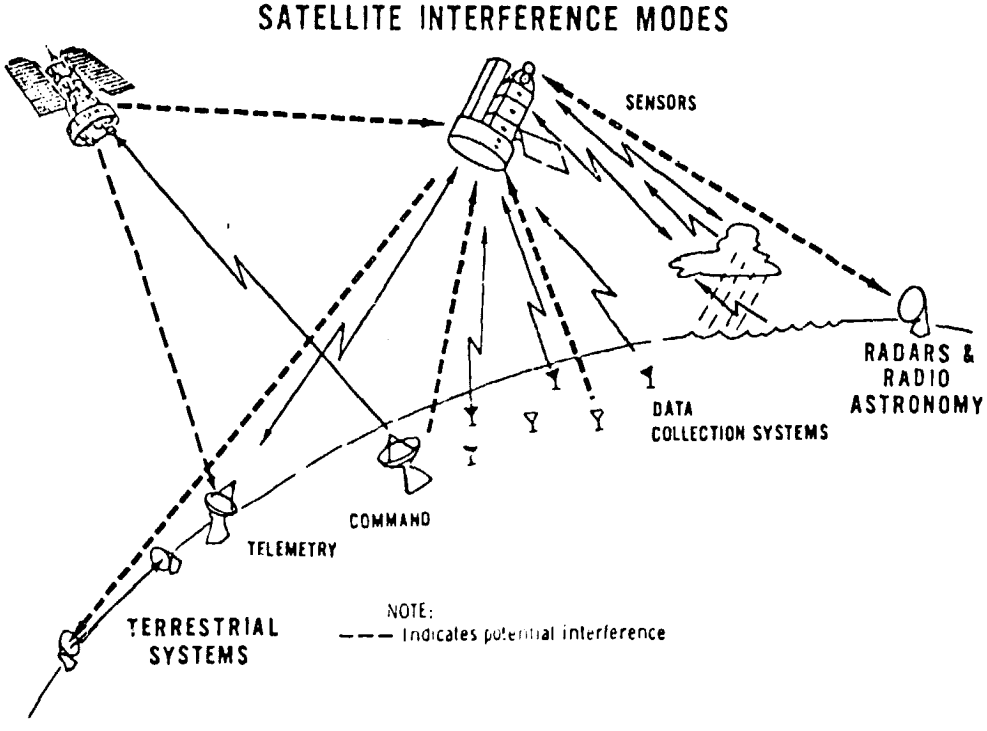

FIGURE 2.0-1b

COMPARISON OF SPACE AND TERRESTRIAL FREQUENCY ALLOCATIONS (BELOW 15 GHz)

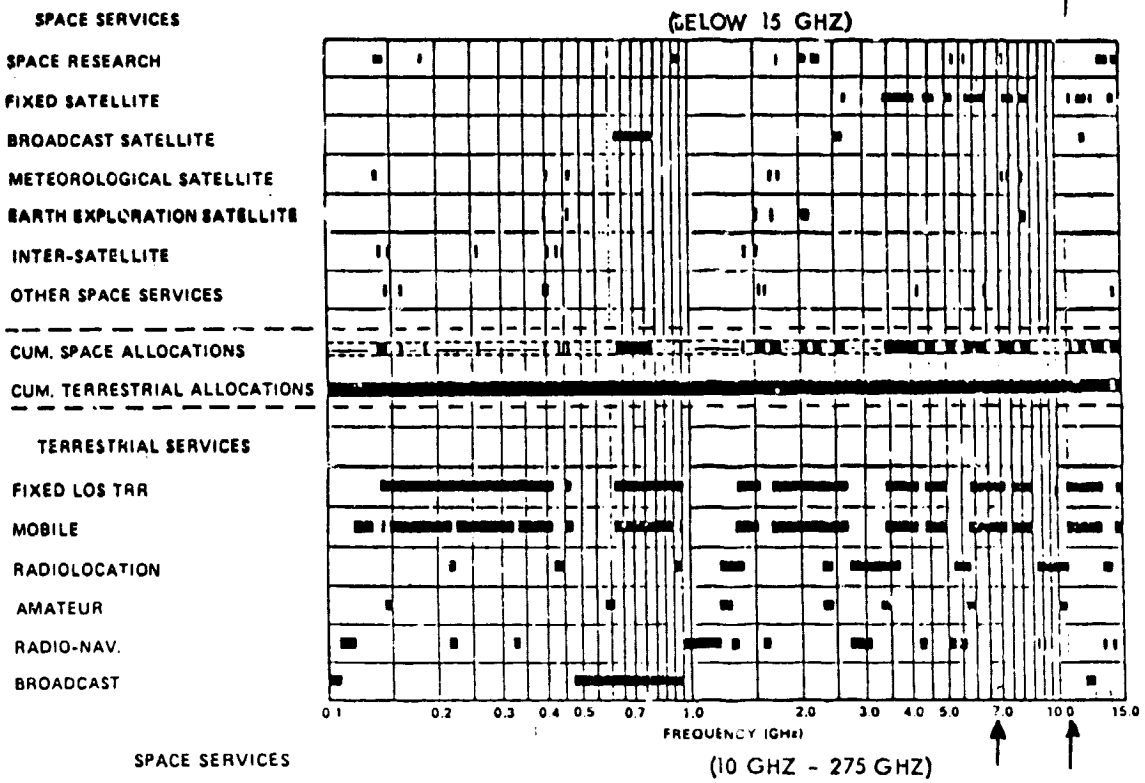

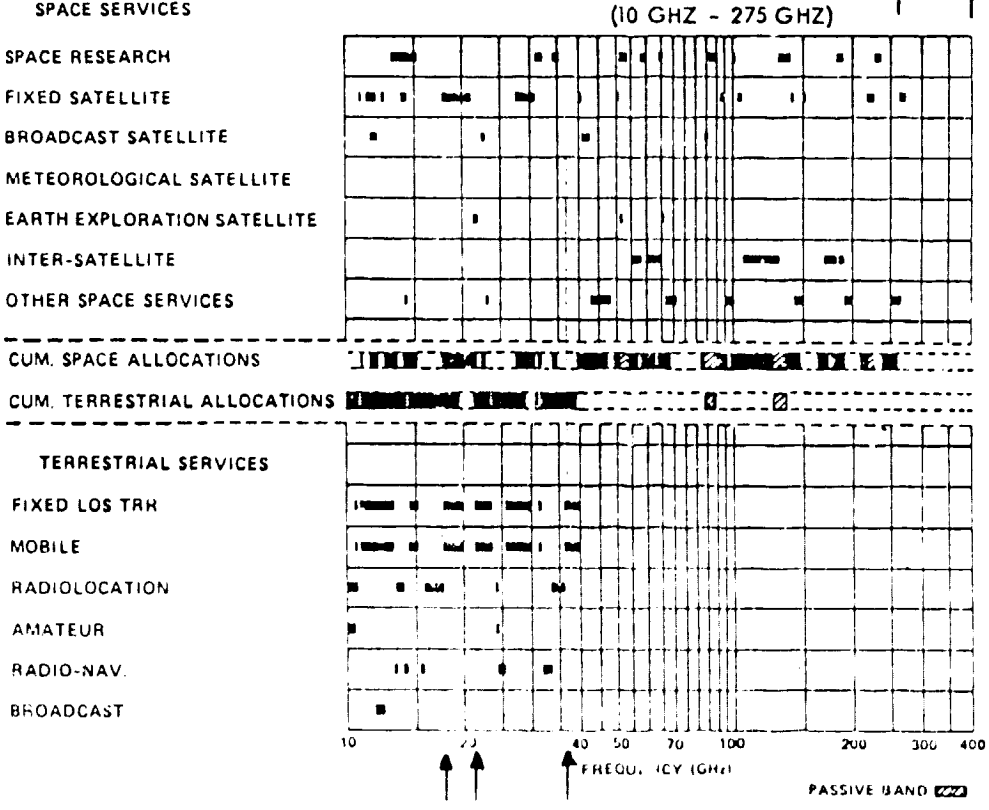

TABLE 2.0-I. SMMR DATA AVAILABLE ON THE CELL-ALL TAPES

	1	2	3	4	5	6	7	8	9	10	11	12	13	14	15	16	17	18	19	20	21	22	23	24	25	26	27	28	29	30	31
OCT 1978	0	0	0	0	0	0	0	0	0	0	0	0	0	0	0	0	0	0	0	0	0	0	0	0	1	1	1	1	1	1	1
NOV 1978	1	1	1	1	1	1	1	1	1	1	1	1	1	1	1	0	1	0	1	0	1	0	1	0	1	0	0	0	0	0	0
FEB 1979	0	0	0	0	0	0	0	0	0	0	0	0	0	0	1	0	*	0	1	0	1	0	1	0	1	0	1	0			
MAR 1979	1	0	1	0	1	0	1	0	1	0	1	0	1	0	1	0	1	0	0	0	0	0	0	0	0	0	0	0			

0 - No Data
1 - Data
* - Bad Data

were used in this task.

To retrieve sea surface temperatures, from the SMMR brightness temperature observations the algorithms developed by (Wilheit and Chang, 1980) were used. These algorithms fit the geophysical parameters as a function of the measured SMMR brightness temperatures and the angle at which the SMMR views the earth (incidence angle). The coefficients for these equations were determined using statistical regression techniques. The retrieved sea surface temperature is computed using the incidence angle and the vertically and horizontally polarized brightness temperatures at all five frequencies at the 156 km antenna resolution.

The SMMR T_b's are also used in an algorithm which approximates rain rate measurements which are used primarily to screen sea surface temperature retrieval for excessive rain. The achievable accuracies of these algorithms are about 1.5° C for SST when the wind speed is greater than 7 m/sec; and 1.0°C for SST at wind speeds less than or equal to 7 m/sec. (Wilheit and Chang, 1980).

To determine the spatial and temporal extent to which severe radio frequency interference affects the SMMR ocean observations, a computer search was made to identify occurrences of intense RFI in the available SMMR data. Sea surface temperatures were computed for all SMMR observations during the November-December 1978, and February-March 1979 time period that were flagged as ocean data on the CELL-ALL tapes. In addition, the rain rate was computed for all the cells in the 780 x 780 km observation block. Tables of brightness temperatures and SST, and maps of the SST overlayed on the earth surface were produced if the following criteria were met.

1. The latitude of the cell was between 50°N and 50°S.
2. The computed rain rate for all the cells in the 780 km x 780 km observation block was less than 1 mm/hr.
3. The sea surface temperature for at least one cell in the 780 km x 780 km block was greater than 50°C.

The first criteria eliminated observations of sea ice, and the second screened SST computations which may be anomalous due to heavy rain in the observation area. The third condition was used to identify occurances of RFI. Since normal sea surface temperatures range from about 10°C to 30°C, SST values greater than 50°C are due to terrestrial transmitters contributing energy to the field of view

as seen by the SMMR antenna. The maps produced for the observations which met these criteria were then checked to see if the SST observation was high because the SMMR antenna may have been partially viewing land. This was done by requiring that the center of the cell containing a SST greater than 50°C be more than 78 km (½ the 156 km cell size) from the nearest land.

Sample maps of SMMR SST observations which satisfy these criteria and are thus instances of RFI, are given in Figure 2.0-2 and 2.0-3. Figure 2.0-2 show the 156 km SST values for an intense RFI observation near the Canary Islands. The 156 km resolution sea surface temperatures are represented by the block of 25 SST values arranged in a 5 x 5 array between 30°N and 38°N latitude and 13°W and 23°W longitude. Land areas are cross hatched in this map. The sea surface temperatures range from 8.4°C to 235.4°C. The maximum SST is well over 50°C, less than 50°N latitude and further than one half a 156 km cell size from land. The 0.0 at about 37.8°N and 14.2°W indicates that the maximum rain rate for this 780 by 780 km block was less than 1 mm/hr, so all the criteria for the presence of RFI were satisfied by this observation. In addition to the SST value of 235.4°C in the cell at 31.1° N and 16.5°W we see that the SST values for the cells on both sides are above 50°C, indicating extended and severe interference with the SST retrieval. By contrast typical SST retrievals free from RFI are observed in the northwest portion of the 5x5 array and have SST values near 23°C.

Figure 2.0-3 shows another RFI occurrence off the coast of California. The maximum SST for this case is only slightly above 50°C, but still considerably larger than the values in neighboring cells.

Thirty-five separate cases of intense RFI were found during the 42 day time period. The anomalously high sea surface temperatures computed for these cases ranged from 50.1°C to 235.4°C. Twenty-nine of the RFI cases occurred during local day and six during local night. Figure 2.0-4 shows the position of each of the intense RFI observations found in the test data. In several geographical areas RFI occurrences are seen repeatedly. These include coastal areas near the northwest coast of Africa near the Canary Islands, near the west coast of the United States, near the Galapagos Islands off the west coast of South America and in the Indian Ocean off the east coast of Africa. These repeated occurrences of high SST's in the same geographical area support the idea that these are observations of

FIGURE 2.0-2. SMMR SST MAP SHOWING RFI NEAR THE CANARY ISLANDS OCT 29, 1978
$12^h\ 31^m\ 45^s$ GMT SST is in (°C)

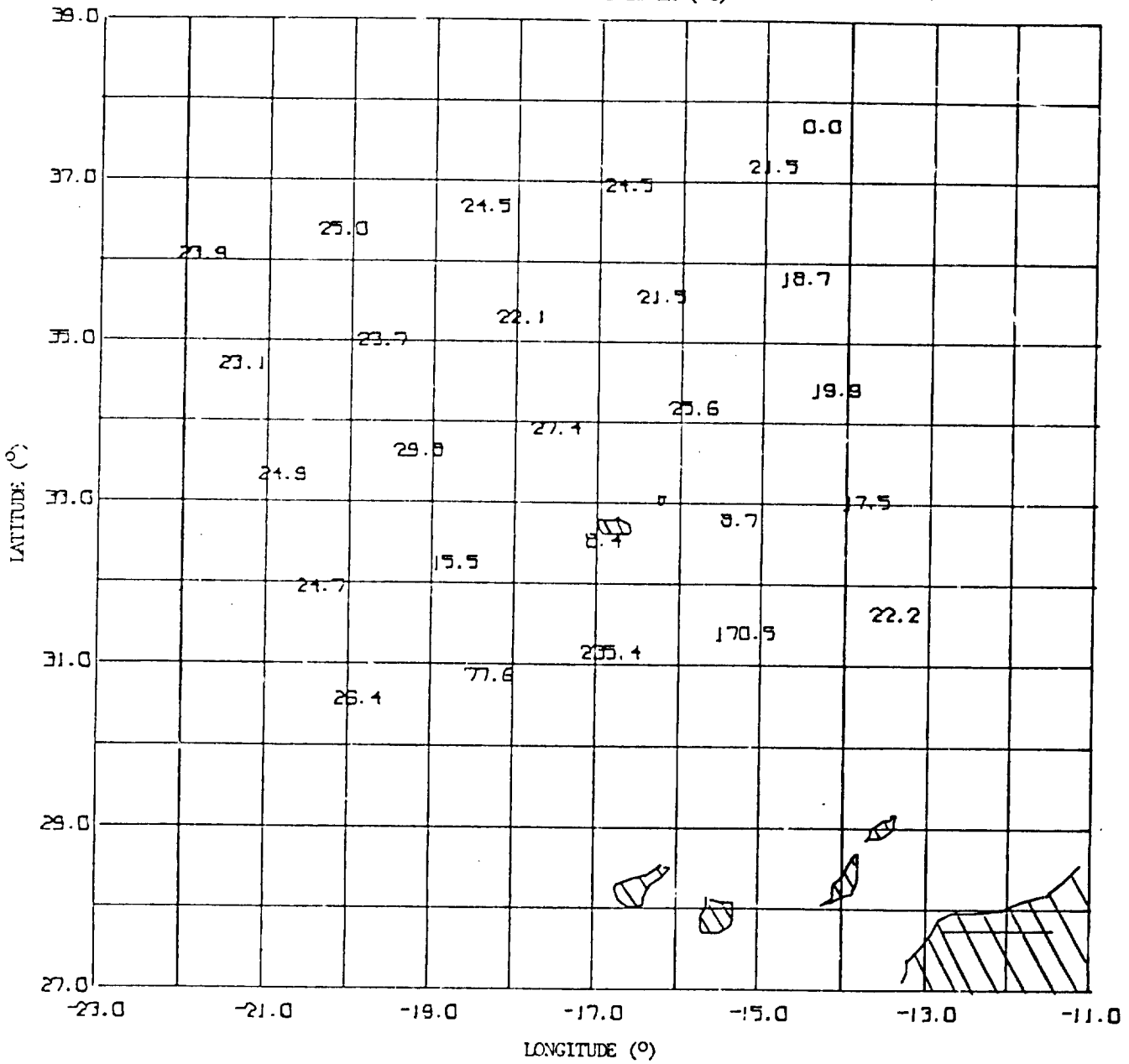

FIGURE 2.0-3. SMMR SST MAP SHOWING RFI OFF CALIFORNIA OCT 29, 1978

$19^h\ 29^m\ 42^s$ SST IS IN (°C)

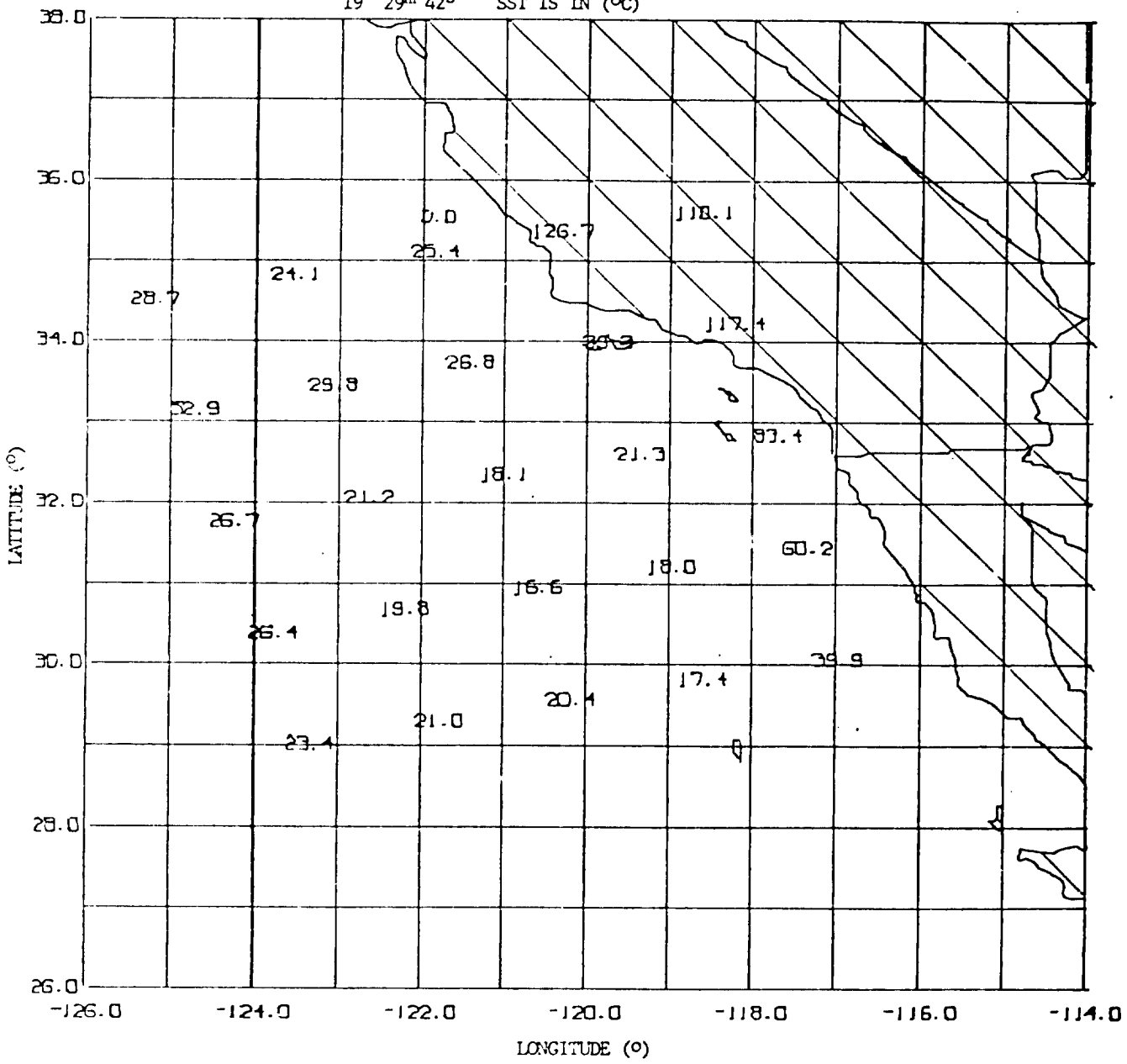

FIGURE 2.0-4

NIMBUS-7
SMMR SEA SURFACE TEMPERATURE OBSERVATIONS
SHOWING SST VALUES ≥ 50°C

OCT 25 - NOV 25, 1978
FEB 15 - MAR 17, 1979

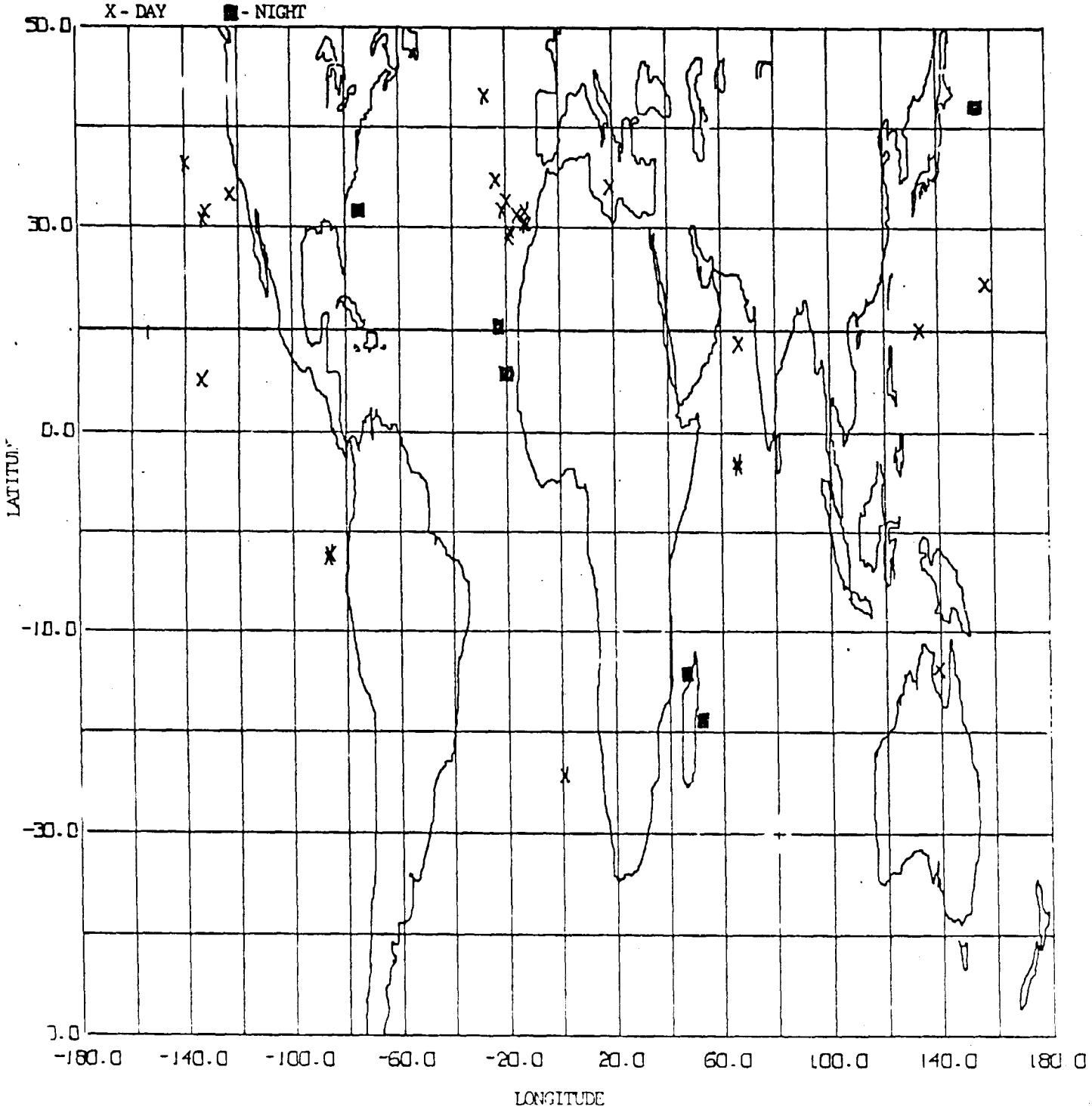

terrestrial RFI, since other causes of abnormally high SST values such as spacecraft telemetry malfunctions or processing problems would not occur consistently in specific geographical areas.

Table 2.0-II gives detailed information on the thirty-five ocean RFI occurrences found in the SMMR data including the date and time of the observation, its latitude and longitude, the vertical and horizontal components of the 6.6 GHz brightness temperature the 6.6 GHz percentage polarization, and the computed sea surface temperature. When the brightness temperatures for these RFI occurrences were examined, it was found that the vertical component of the 6.6 GHz brightness temperature was always higher than the mean ocean values of about 160°K. Considerably less perturbation was seen in the 6.6 GHz horizontal component. The brightness temperatures at the four other frequencies were all very close to their mean ocean values.

In addition to identifying isolated intense point sources of strong radio frequency interference, it is also important to determine how less intense RFI may affect SMMR retrieval of sea surface temperatures over broader areas of the ocean. To begin to understand this problem comparisons were made between SMMR SST retrievals, and SST observations from an instrument which is not affected by terrestrial radio transmitters.

Sea surface temperature data for February and March 1979 was available from the Advanced Very High Resolution Radiometer (AVHRR) flown aboard the TIROS-N spacecraft. The AVHRR is a 4 channel scanning radiometer sensitive in four spectral regions in the visible, near infrared, and infrared bands. By combining the readings for the AVHRR's infrared channels, sea surface temperatures can be computed taking into account the effect of clouds. The AVHRR provides 50 km resolution SST measurements with an expected standard deviation of the noise level in the infrared channels of about 0.2°C. The AVHRR SST's are available on seven day data tapes with the 50°km resolution SST's put in 1° latitude/longitude blocks.

For this study, eight 20° latitude by 30° longitude ocean/coast areas near North America, South America, Australia and Africa were chosen for analysis. Figure 2.0-5 shows a map of these areas. These areas were chosen to allow examination of ocean data to both the east and west of land, to include areas in

TABLE 2.0-II

NIMBUS-7

SMMR SEA SURFACE TEMPERATURE OBSERVATIONS

SHOWING INTENSE RADIO FREQUENCY INTERFERENCE

OCT 25 - NOV 25, 1978

SEA SURFACE TEMPERATURES GREATER THAN 50°C

OBSERVATIONS GREATER THAN 78 km FROM NEAREST LAND

OBSERVATION	DATE	DAY/NIGHT	GMT SECONDS OF DAY	LATITUDE(°)	LONGITUDE(°)	6.6 GHz MEASUREMENTS T_{bV}(°K)	T_{bH}(°K)	P%	SST(°C)
1	10/29/78	D	26038	6.5	65.1	179.2	96.2	30.1	76.0
2	10/29/78	D	45103	30.2	-12.9	183.0	116.2	22.3	70.7
3	10/29/78	D	45225	31.1	-16.5	229.4	95.7	41.1	235.4
4	10/29/78	D	70182	33.1	-124.6	169.6	95.5	21.0	52.9
5	10/30/78	D	64362	-2.3	-87.6	178.8	89.5	33.3	87.5
6	11/03/78	D	25228	18.7	66.1	172.8	92.1	30.5	64.5
7	11/04/78	D	45181	30.2	-14.6	203.0	98.8	34.5	150.9
8	11/07/78	N	6804	20.2	-24.7	168.7	92.9	29.0	52.0
9	11/08/78	D	43167	30.7	-11.3	176.4	98.9	28.2	63.4
10	11/11/78	D	46244	28.8	-20.4	184.6	101.2	29.2	92.7
11	11/11/78	D	64471	-2.5	-87.7	173.9	92.2	30.7	69.9
12	11/11/78	N	74143	-14.4	46.2	191.1	101.2	30.8	104.7
13	11/15/78	D	44266	32.0	-11.1	170.7	89.6	31.2	62.9
14	11/15/78	D	75544	36.2	-140.8	166.7	86.2	31.8	54.3
15	11/17/78	D	46303	29.4	-19.1	175.4	95.4	29.5	72.4
16	11/19/78	D	4584	24.8	157.3	185.4	96.2	31.7	96.8
17	11/19/78	D	73479	31.4	-134.2	171.3	93.1	29.6	63.0
18	11/21/78	N	72171	-19.0	51.7	169.5	99.2	28.6	53.8
19	11/23/78	D	64586	-2.8	-88.1	169.1	92.0	29.5	53.1
20	11/25/78	D	10188	-14.8	140.4	176.9	100.8	27.4	60.5
21	11/25/78	D	73435	30.6	-134.3	175.8	96.2	29.3	73.8

TABLE 2.0-II (Cont'd)

NIMBUS-7
SMMR SEA SURFACE TEMPERATURE OBSERVATIONS
SHOWING INTENSE RADIO FREQUENCY INTERFERENCE

FEB 15 - MAR 17, 1979

SEA SURFACE TEMPERATURES GREATER THAN 50°C
OBSERVATIONS GREATER THAN 78 km FROM NEAREST LAND

OBSERVATION	DATE	DAY/NIGHT	GMT SECONDS OF DAY	LATITUDE(°)	LONGITUDE(°)	6.6 GHz MEASUREMENTS T_{bV}(°K)	T_{bH}(°K)	P%	SST(°C)
22	2/19/79	N	5537	15.9	-19.8	168.5	93.9	28.4	50.1
23	2/21/79	D	47020	31.6	-22.2	178.5	110.9	23.4	69.5
24	2/21/79	D	36676	34.0	18.5	169.8	94.5	28.5	54.4
25	2/21/79	D	73917	15.0	-135.7	188.1	89.0	35.8	116.4
26	2/23/79	D	44075	-24.4	-0.3	179.8	93.7	31.5	85.0
27	2/25/79	D	9568	20.0	132.8	170.6	95.4	28.3	53.8
28	3/01/79	D	26267	6.9	64.5	170.0	89.3	31.1	60.1
29	3/01/79	D	45334	30.4	-13.6	170.6	92.5	29.7	59.8
30	3/07/79	D	45681	32.5	-20.6	223.1	99.9	38.1	210.5
31	3/09/79	D	47880	32.3	-24.5	169.9	91.3	30.1	61.3
32	3/09/79	D	48002	34.6	-28.6	169.8	88.2	31.6	64.3
33	3/09/79	N	49720	43.1	155.3	173.4	86.8	33.3	76.1
34	3/11/79	D	43979	41.8	-14.2	173.8	91.5	31.0	74.6
35	3/15/79	N	19063	31.5	-77.5	173.2	95.5	28.9	62.1

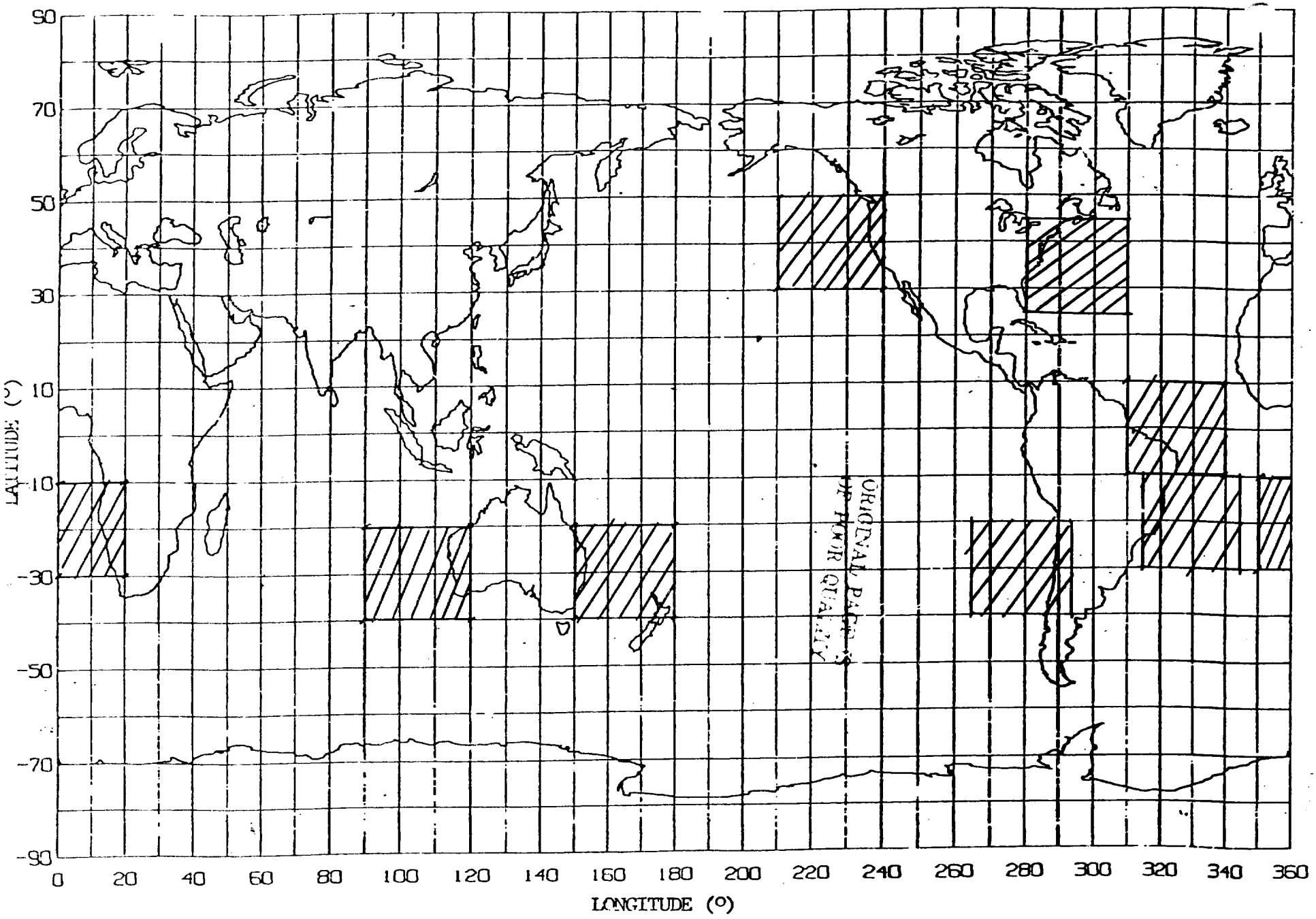
SMMR-AVHRR $\overline{SST}$ COASTAL COMPARISON AREAS
90
70
50
30
10
-10
-30
-50
-70
-90
LATITUDE (°)
0
20
40
60
80
100
120
140
160
180
200
220
240
260
280
300
320
340
360
LONGITUDE (°)

FIGURE 2.0-5

both the northern and southern hemisphere, and to include areas which did and did not contain intense point sources of RFI.

Monthly averages of the SMMR and AVHRR sea surface temperatures for the time period February 15 to March 16, 1979 were computed for every 2° latitude by 2° longitude ocean block in the eight coastal areas. The SMMR SST's were divided into day and night data, and were screened for bad data, and cases of rain rate greater than 1 mm/hr. The February 15 to March 16, 1979 time period was chosen because it was the only time overlapping SMMR and AVHRR data was available.

In addition, the difference between the averaged SMMR SST (SST_S) and AVHRR SST (SST_A) ($\overline{\Delta SST}$) was computed for the 2° by 2° ocean blocks in each coastal area. Here $\overline{\Delta SST}$ is defined by

$$\overline{\Delta SST} = \overline{SST}_S - \overline{SST}_A$$

Figure 2.0-6 to Figure 2.0-37 show the $\overline{\Delta SST}$ for each 2° by 2° block mapped and contoured for each of the eight coastal areas. The coastal land is cross hatched in the maps and $\overline{\Delta SST}$ values of 0.0 indicate blocks in which there is no data. To eliminate any cases in which the SMMR field of view included both land and ocean, the 2° by 2° block which included the coast as well as the next block in the direction of the open ocean were constrained to have no data. Coastal blocks with no data were ignored when the contours were produced. If there is a block with no data in the open ocean portion of the map, an interpolated $\overline{\Delta SST}$ value was put in if there was valid data in three of the four nearest neighboring blocks. The contour lines are at intervals of $2^{\circ}C$.

Since each test area is 30° in longitude wide, $\overline{\Delta SST}$ values are available near the coast ($\sim 4^{\circ}$-6° from land) as well as far from the coast ($\sim 22^{\circ}$-24° from land) in the open ocean. Comparing average SSMR and AVHRR SST values through $\overline{\Delta SST}$ can give a picture of the effect of radio frequency interference from land based transmitters in coastal ocean areas. RFI from fixed site land based transmitters would not affect the SMMR data in the open ocean far from land. Thus $\overline{\Delta SST}$ values far from land in the open ocean represent the way that SMMR and AVHRR sea surface temperatures compare when the SMMR data is free from RFI effects. Since the AVHRR SST retrievals are based on infrared measurements, microwave RFI of course would not affect them. If we assume that the AVHRR sea surface temperatures remain relatively constant to within 2° or $3^{\circ}C$ in the test area; which

is generally the case; then $\Delta\overline{SST}$ values more than 2^{o} or 3^{o} higher than the open ocean values are due to increases in the SMMR sea surface temperatures. Systematic increases in $\Delta\overline{SST}$ of more than a few degrees as we move from open ocean to the coast then indicate the presence of radio frequency interference with SMMR in the coastal ocean.

Of the eight coastal areas where $\Delta\overline{SST}$ was examined, all showed evidence of systematic increase in $\Delta\overline{SST}$ for at least the day or night data. There are differences however between the $\Delta\overline{SST}$ signature in the test areas, primarily in the amount which $\Delta\overline{SST}$ changed in going from open ocean to the coast. In several cases such as the east coast of North America at night, the west coast of Australia at day, the west coast of South America at day, and the west coast of southern Africa at night, the differences between open ocean and near coastal values of SST were quite dramatic. In each of these cases lines of constant $\Delta\overline{SST}$ closely parallel the coastline and decrease nearly monatonically with distance from land, and the near coast values of $\Delta\overline{SST}$ were more than 10^{o}C larger than open ocean values. In addition the contour maps for two of these areas show regions high and rapidly changing $\Delta\overline{SST}$ near major coastal population areas, Perth, Australia; and Santiago, Chile, an indication of strong RFI effects.

In three test areas $\Delta\overline{SST}$ stays practically constant in moving from open ocean to the coast. These cases are the east coast of North America at day, the east coast of South America at day, and the northeast coast of South America at night.

In the rest of the test areas, some systematic decrease in $\Delta\overline{SST}$ is observed in moving away from land with open ocean $\Delta\overline{SST}$ levels being reached at distances from land which range from 6^{o} to 22^{o}.

In each of the eight test areas day and night cases were very different in both the magnitude of the $\Delta\overline{SST}$ change from open ocean to land, as well as in the shape of the contour plots. Since the relative scanner/coastline geometry is different during the day and night NIMBUS-7 passes, these day/night differences in $\Delta\overline{SST}$ may reflect the effect of different transmitter-SMMR configurations on the RFI signature. However, since in every one of the eight test cases some systematic increase in $\Delta\overline{SST}$ was observed from open ocean to coast in either day or night data, some other coastline-scanner geometry effect may also be present. A SMMR

antenna sidelobe viewing coastal land, or a coldhorn antenna viewing the earth rather than space are examples of instrument-related causes which could produce such effects. Distortions of $\Delta\overline{SST}$ arising from sources such as these would be superimposed on the RFI signature in the $\Delta\overline{SST}$ data.

FIGURE 2.0-6. DAYTIME $\overline{\Delta SST}$ FOR FEB 15-MAR 16, 1979

$\overline{\Delta SST}$ VALUES FOR WEST COAST OF NORTH AMERICA

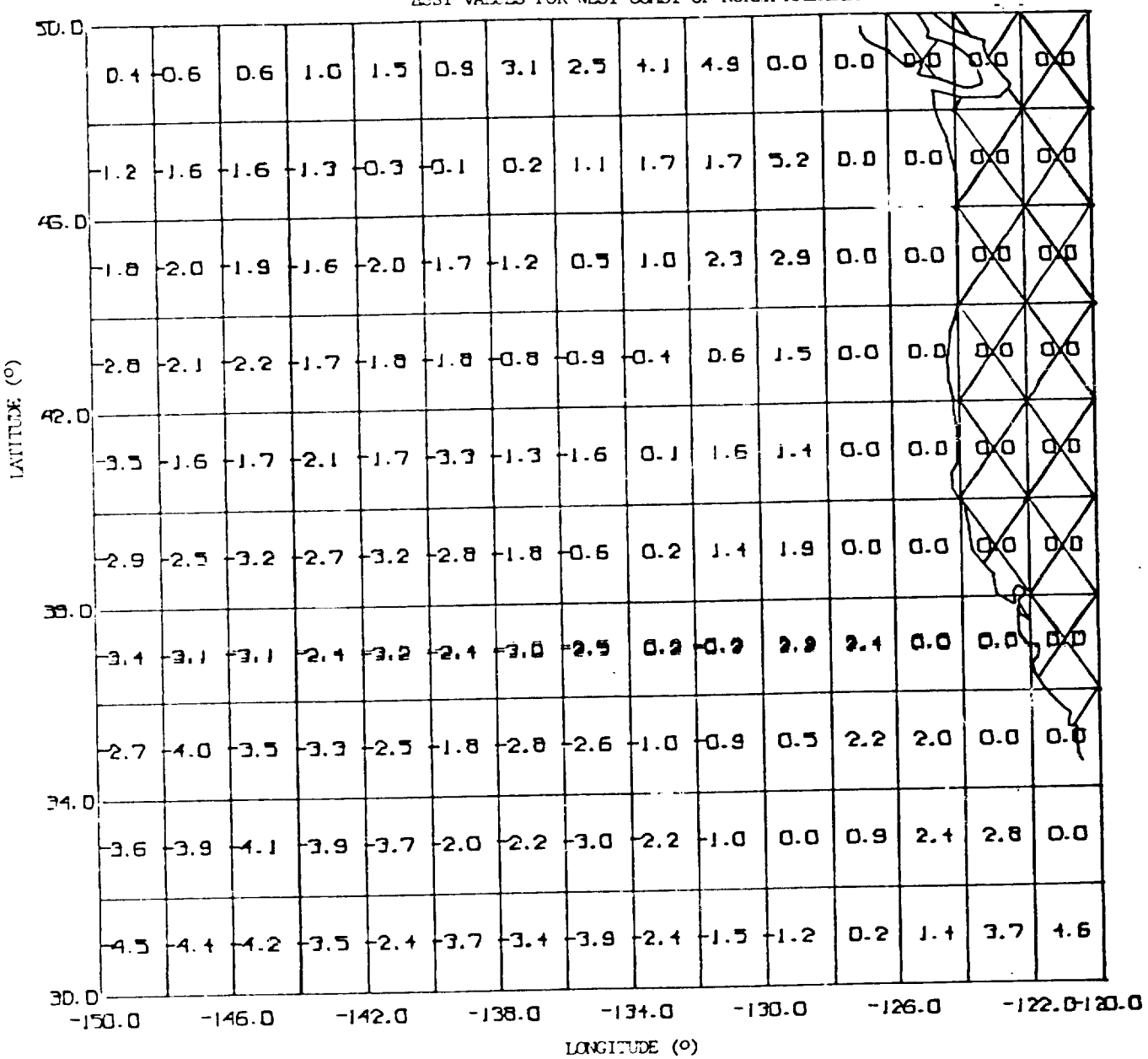

FIGURE 2.0-7. DAYTIME $\Delta\overline{SST}$ FOR FEB 15-MAR 16, 1979
$\Delta\overline{SST}$ CONTOURS FOR WEST COAST OF NORTH AMERICA

Note lines of constant $\Delta\overline{SST}$ running parallel to the coast and decreasing nearly monatonically with distance from land.

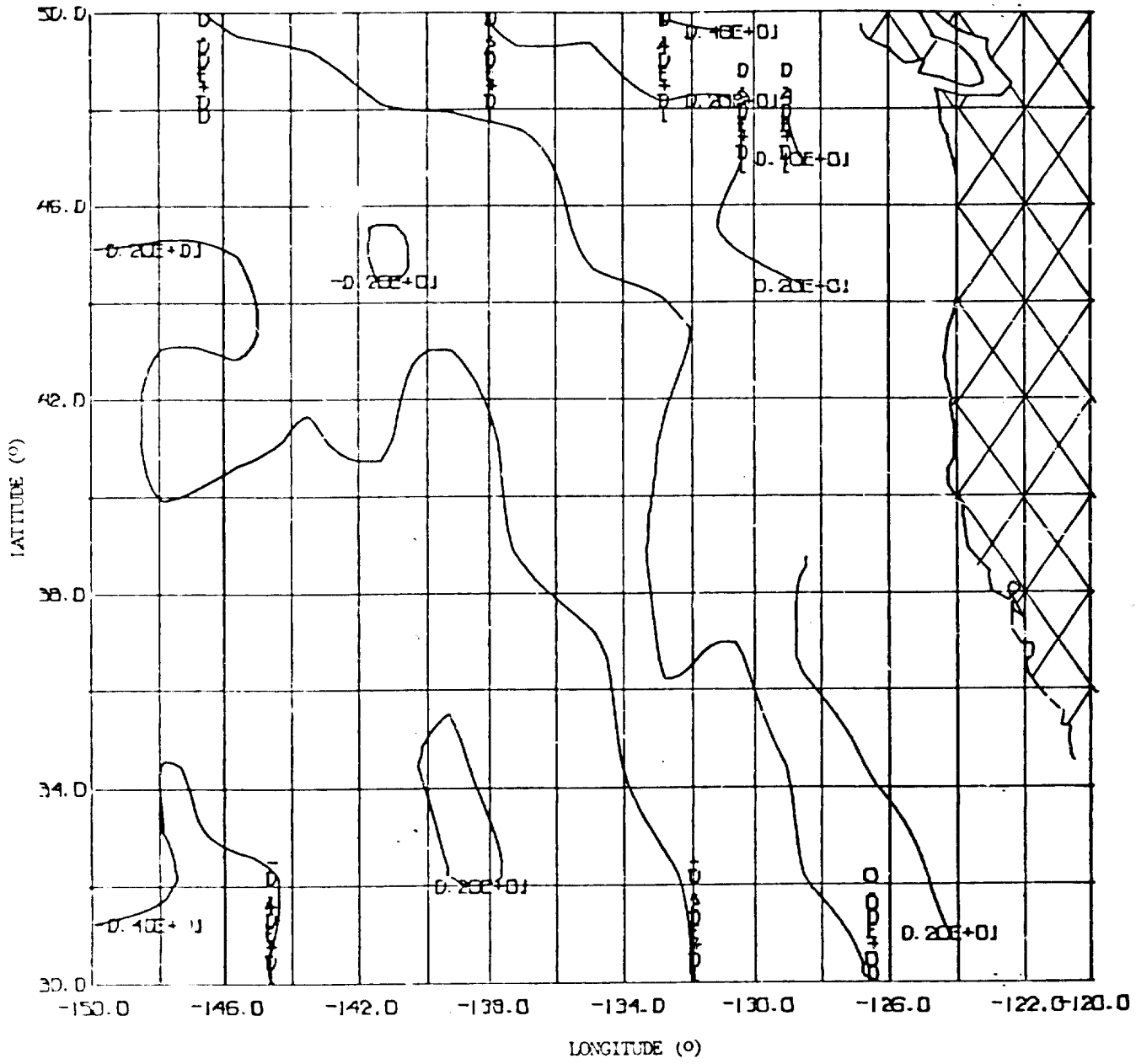

FIGURE 2.0-8. NIGHTTIME $\Delta\overline{SST}$ FOR FEB 15-MAR 16, 1979

$\Delta\overline{SST}$ VALUES FOR WEST COAST OF NORTH AMERICA

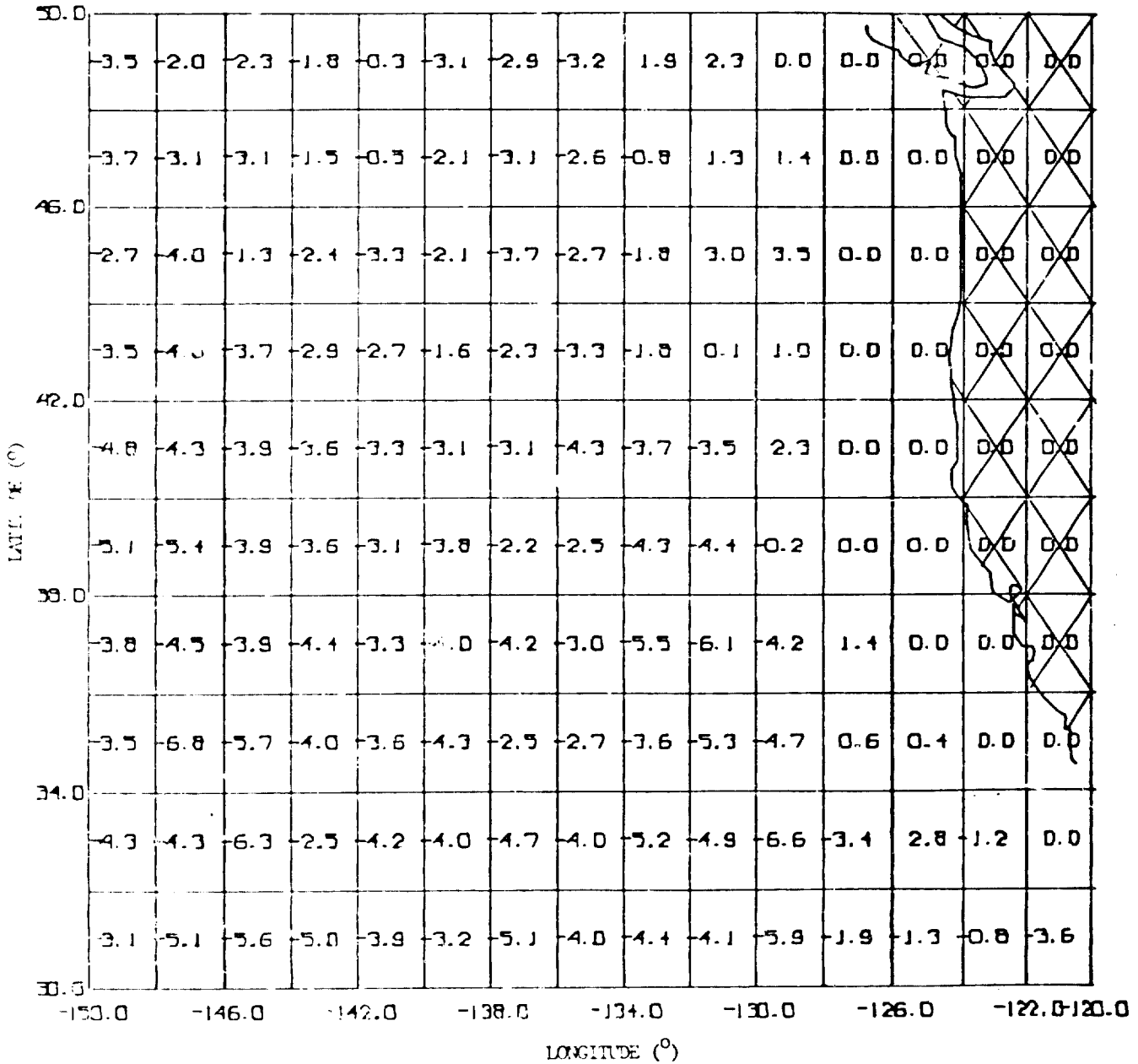

FIGURE 2.0-9. NIGHTTIME $\overline{\Delta SST}$ FOR FEB 15-MAR 16, 1979
$\overline{\Delta SST}$ CONTOURS FOR WEST COAST OF NORTH AMERICA

Note lines of constant $\overline{\Delta SST}$ running parallel to the coast and decreasing nearly monotonically with distance from land

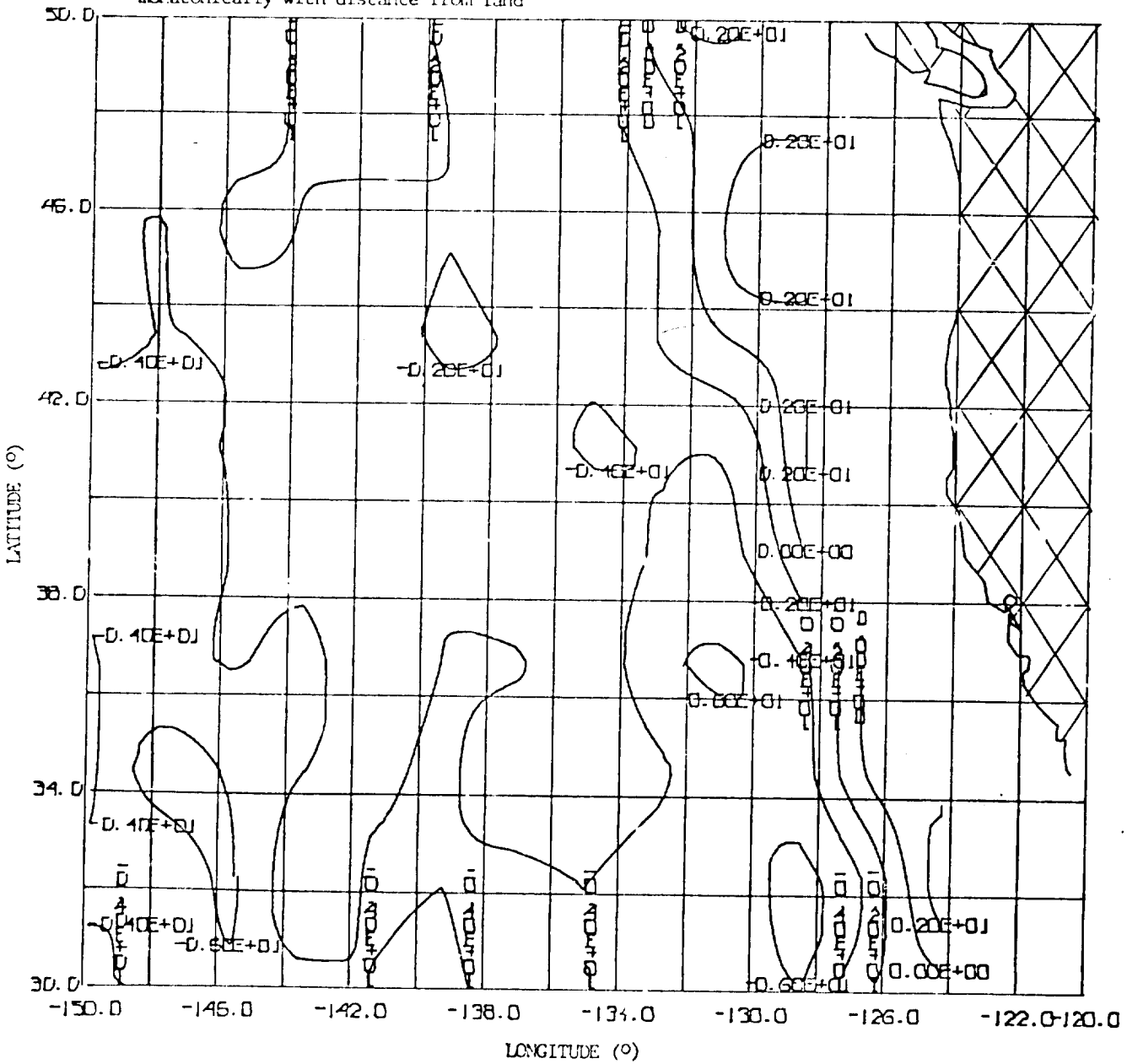

FIGURE 2.0-10. DAYTIME $\overline{\Delta SST}$ FOR FEB 15-MAR 16, 1979
$\overline{\Delta SST}$ VALUES FOR EAST COAST OF NORTH AMERICA

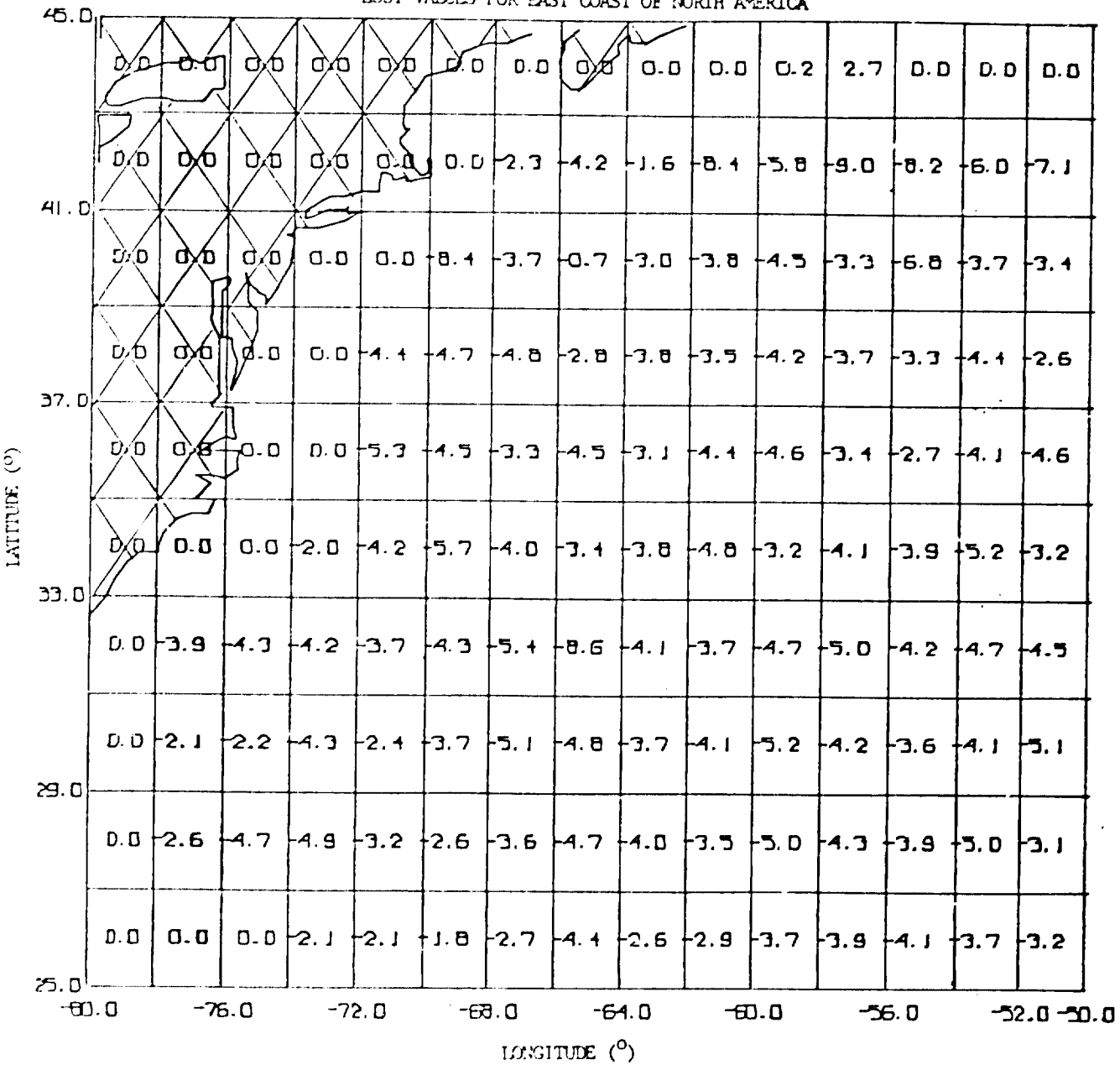

FIGURE 2.0-11. DAYTIME $\Delta\overline{SST}$ FOR FEB 15-MAR 16, 1979

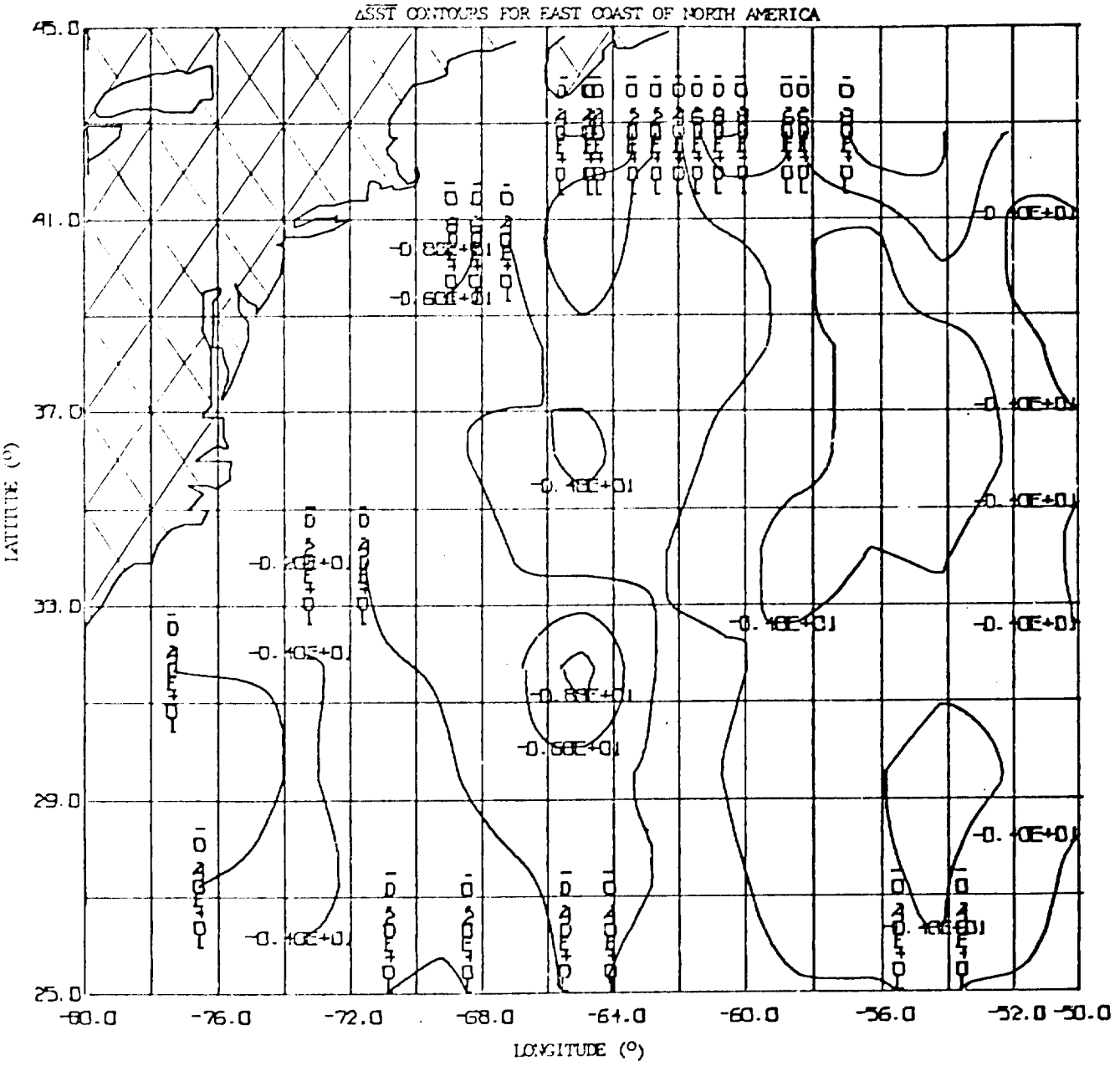

FIGURE 2.0-12. NIGHTIME $\Delta\overline{SST}$ FOR FEB 15-MAR 16, 1979
$\Delta\overline{SST}$ VALUES FOR EAST COAST OF NORTH AMERICA

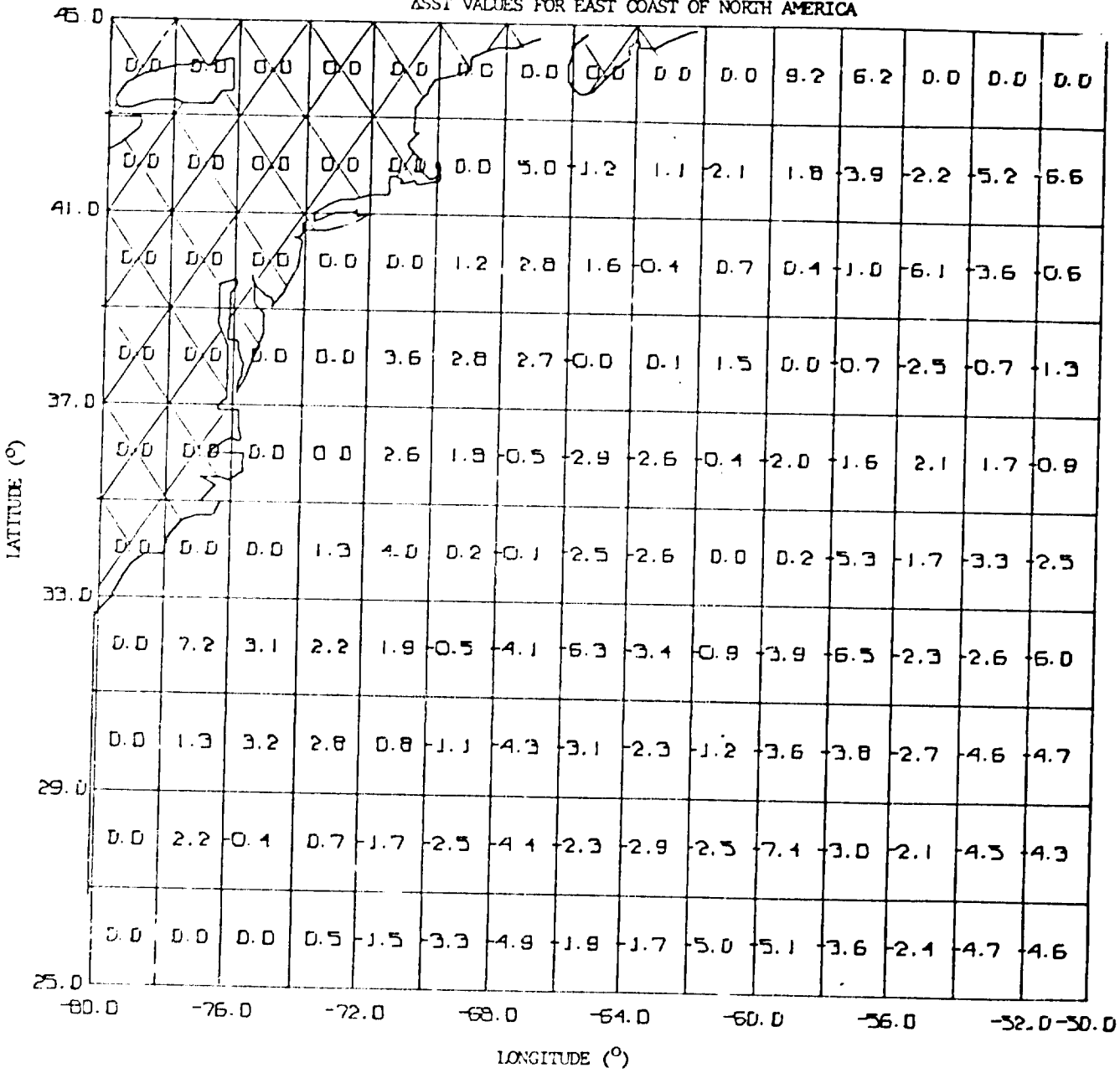

FIGURE 2.0-13. NIGHTTIME $\overline{\Delta SST}$ FOR FEB 15-MAR 16, 1979

$\overline{\Delta SST}$ CONTOURS FOR EAST COAST OF NORTH AMERICA

Note lines of constant $\overline{\Delta SST}$ running parallel to the coast and decreasing nearly monatonically with distance from land.

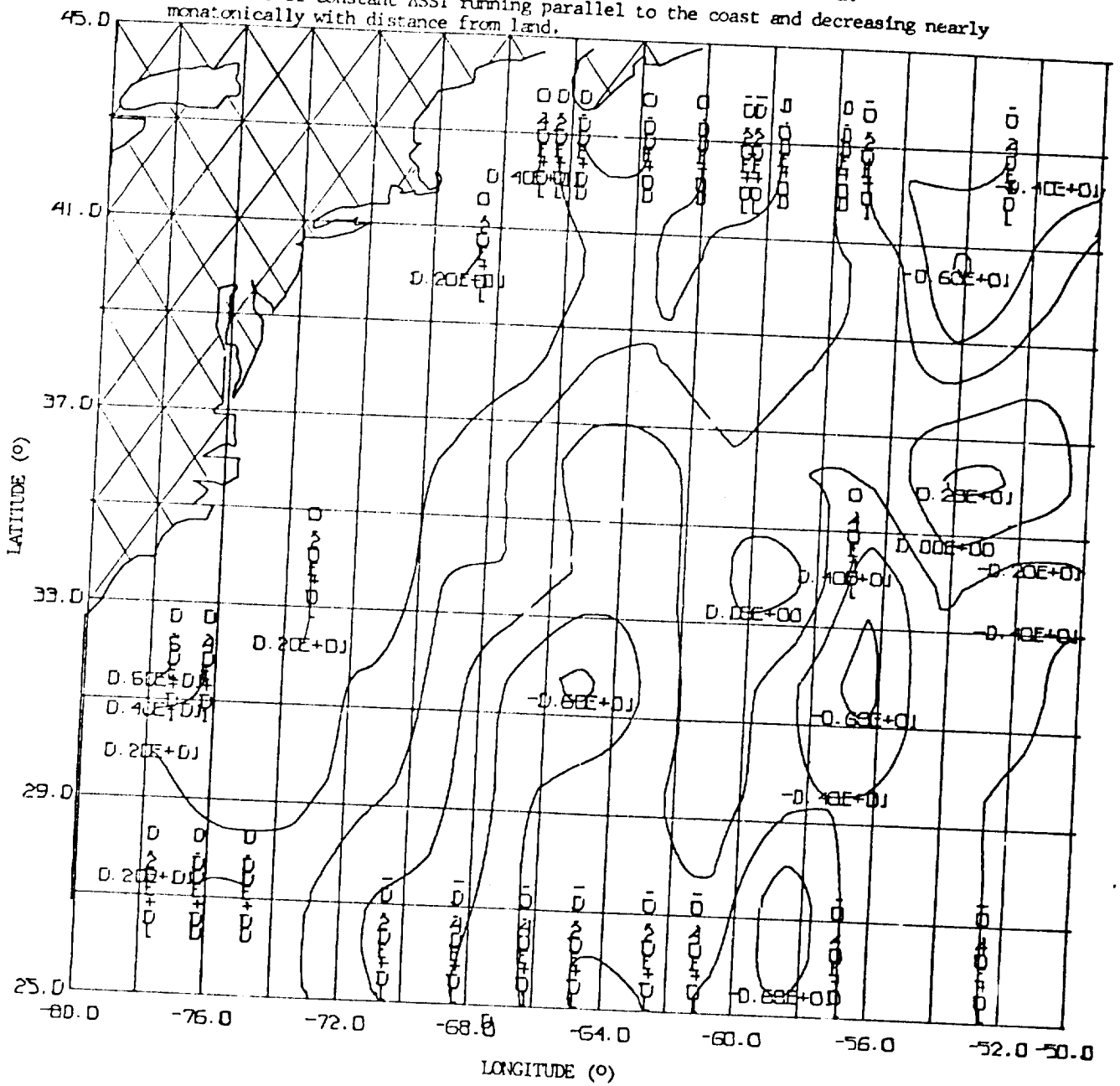

FIGURE 2.0-14. DAYTIME $\Delta\overline{SST}$ FOR FEB 15-MAR 16, 1979

$\Delta\overline{SST}$ VALUES FOR WEST COAST OF AUSTRALIA

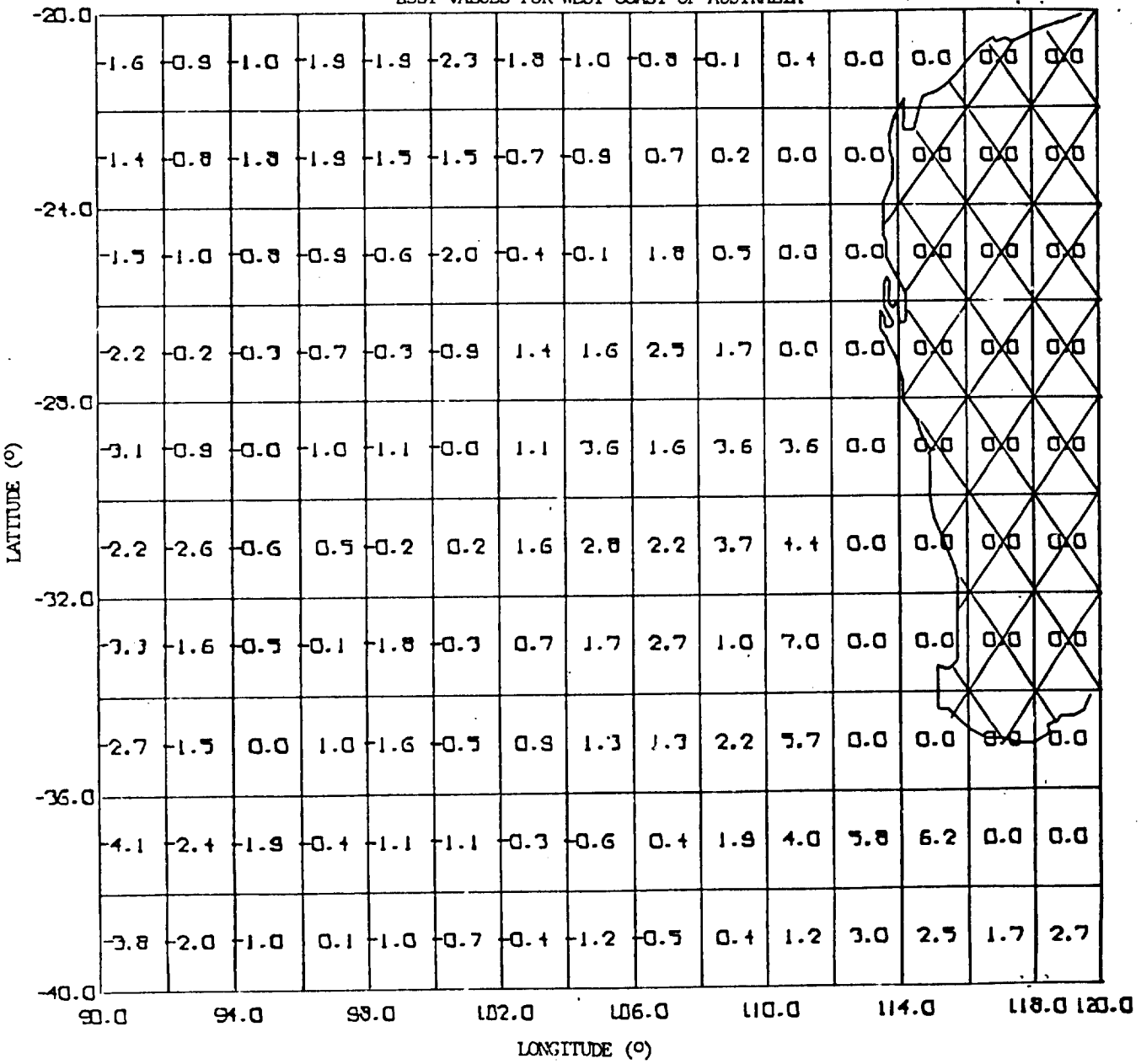

FIGURE 2.0-15. DAYTIME $\Delta\overline{SST}$ FOR FEB 15-MAR 16, 1979
$\Delta\overline{SST}$ CONTOURS FOR WEST COAST OF AUSTRALIA

Note lines of constant $\Delta\overline{SST}$ running parallel to the coast and decreasing nearly monatonically with distance from land.

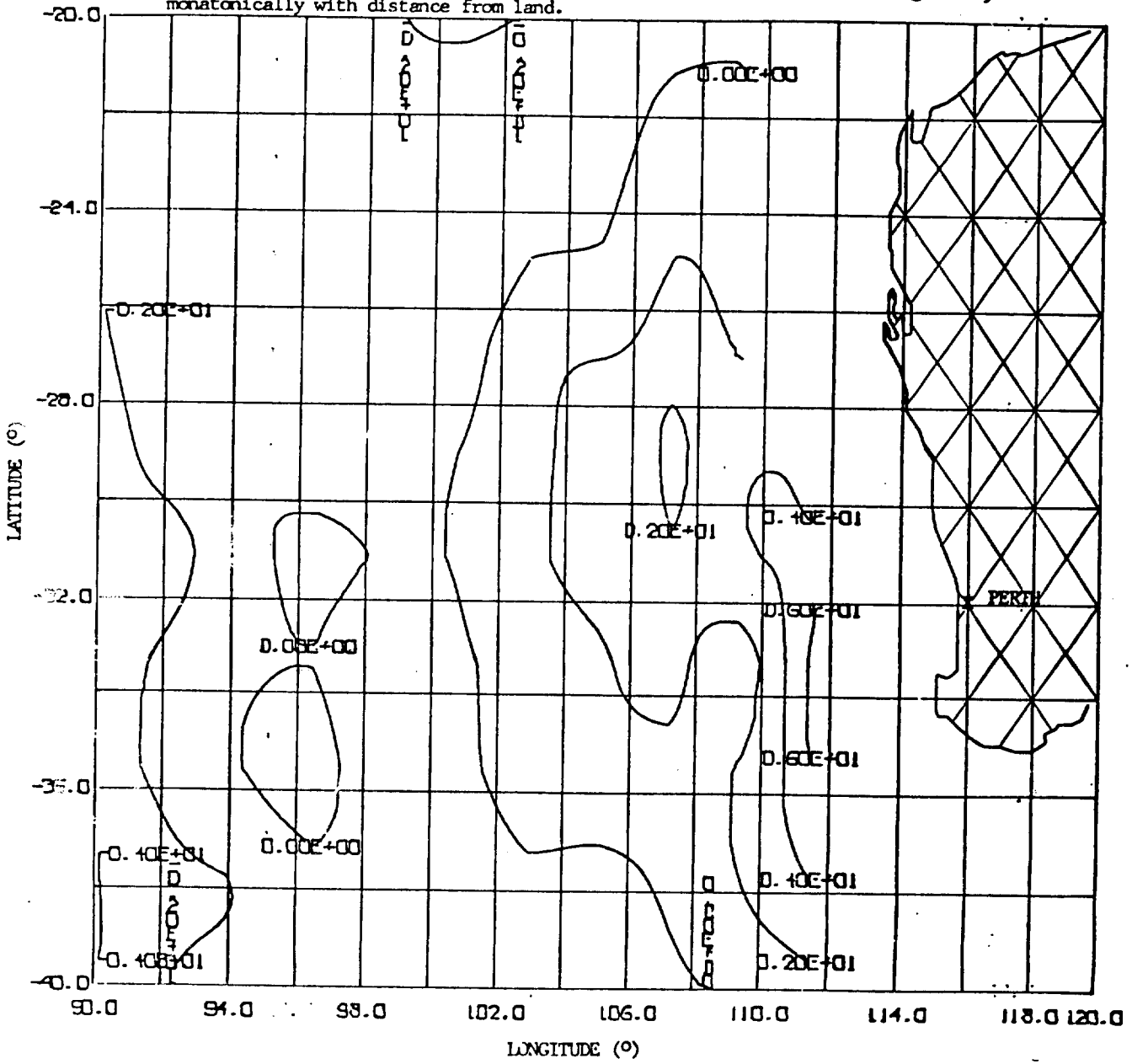

FIGURE 2.0-16. NIGHTTIME $\Delta\overline{SST}$ FOR FEB 15-MAR 16, 1979
$\Delta\overline{SST}$ VALUES FOR WEST COAST OF AUSTRALIA

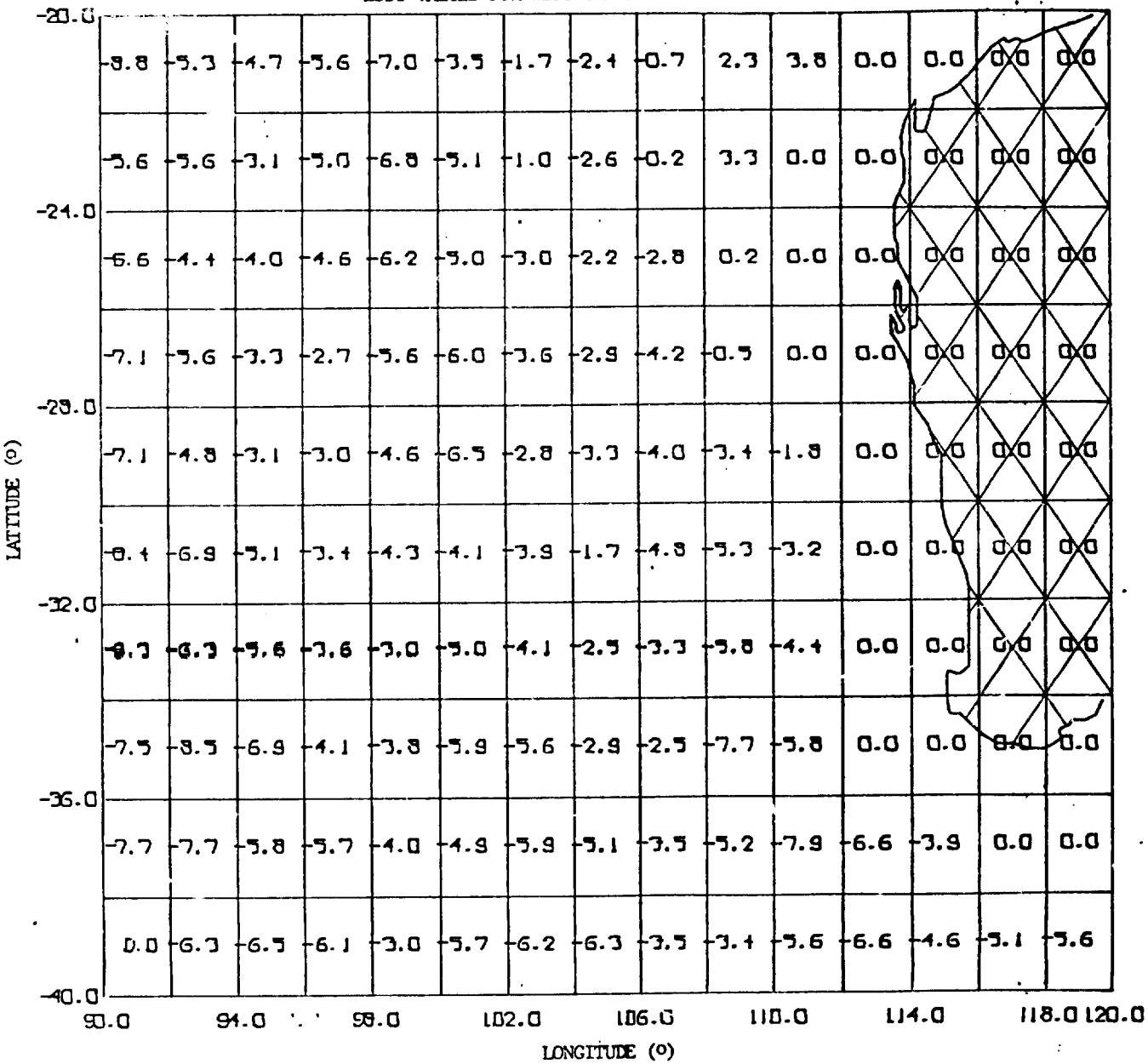

FIGURE 2.0-17. NIGHTTIME $\Delta\overline{SST}$ FOR FEB 15-MAR 16, 1979

$\Delta\overline{SST}$ CONTOURS FOR WEST COAST OF AUSTRALIA

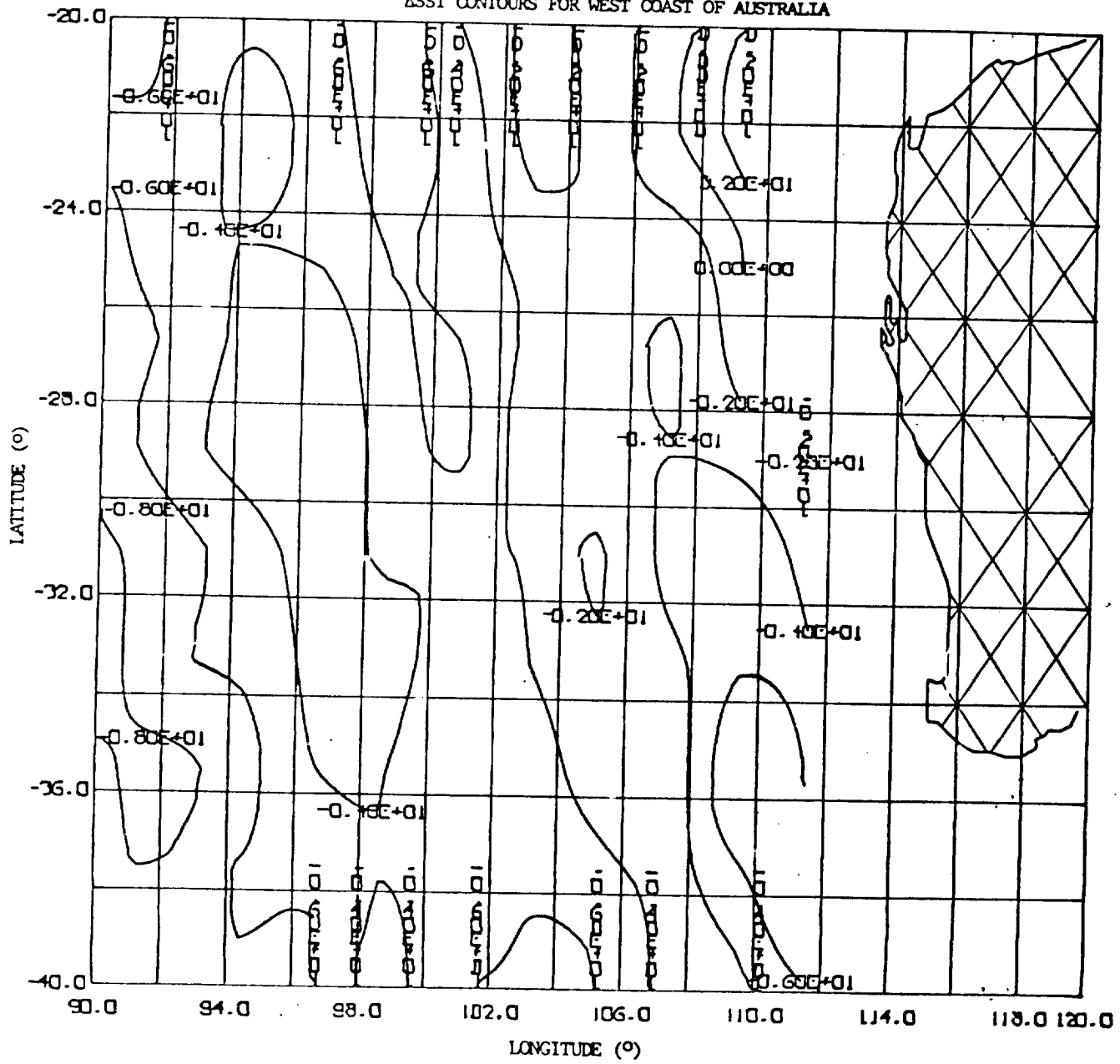

FIGURE 2.0-18. DAYTIME ΔSST FOR PER 15-MAR 16, 1979
ΔSST VALUES FOR EAST COAST OF AUSTRALIA

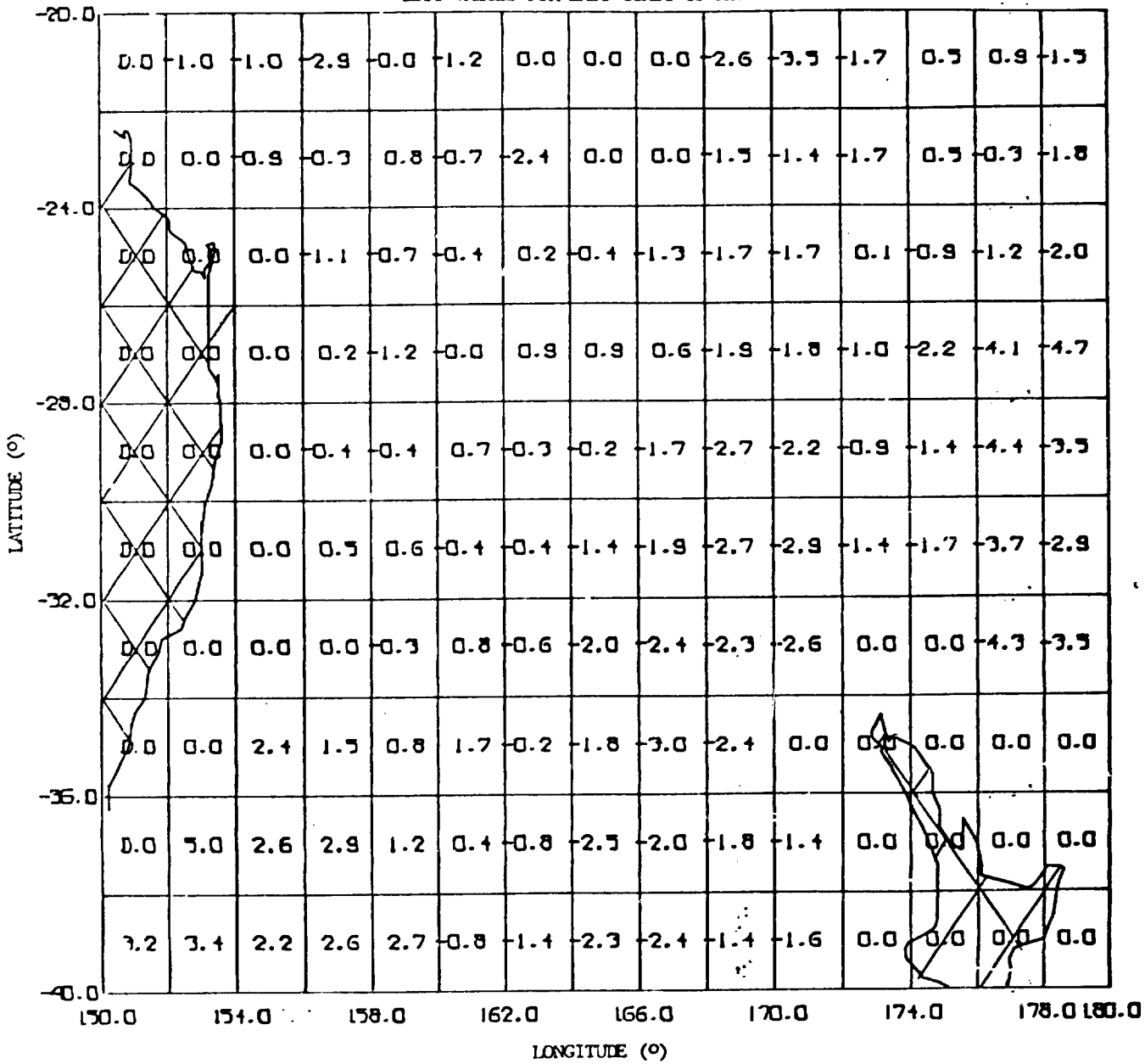

FIGURE 2.0-19. DAYTIME ΔSST FOR FEB 15-MAR 16, 1979
ΔSST CONTOURS FOR EAST COAST OF AUSTRALIA

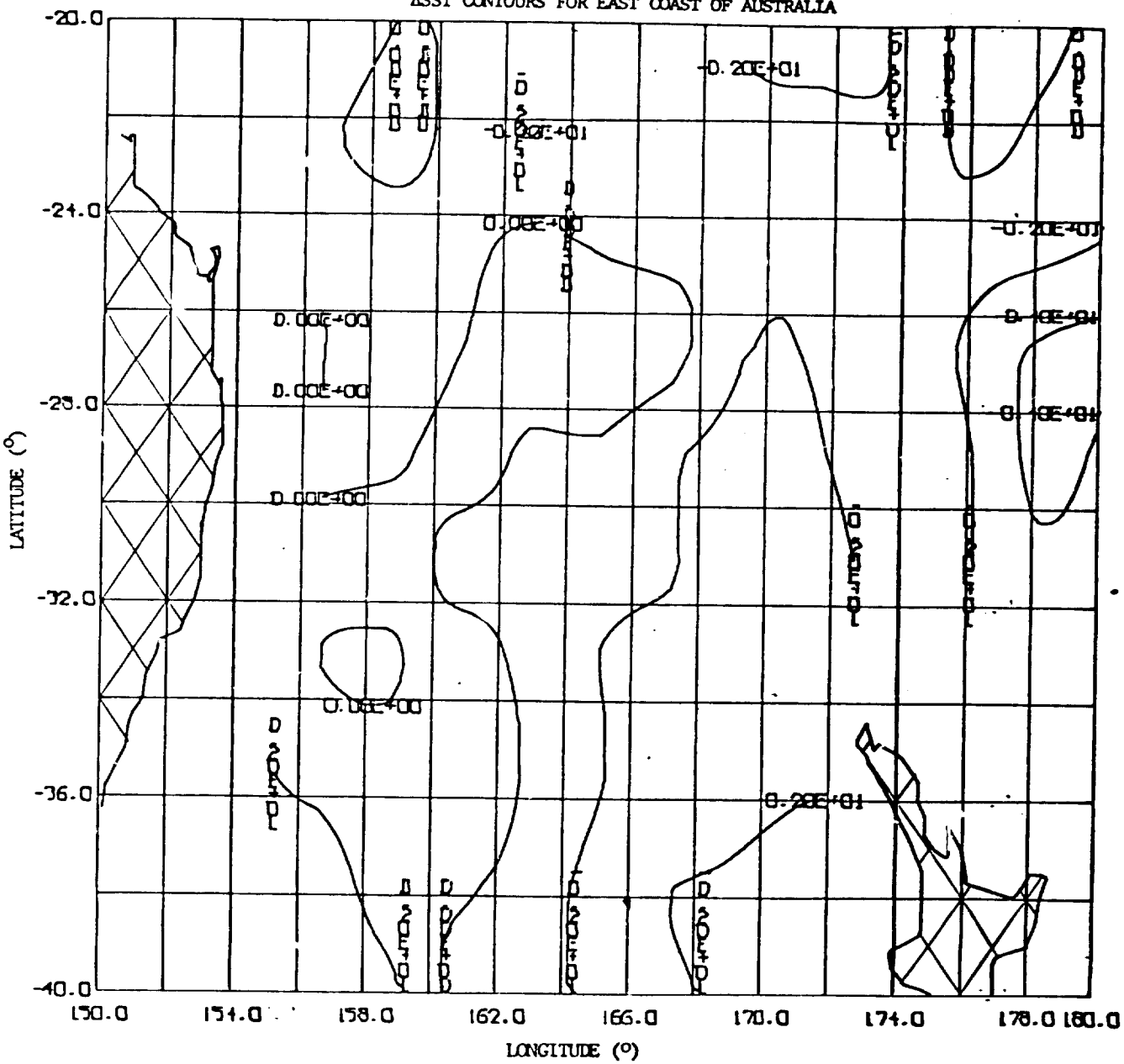

FIGURE 2.0-20. NIGHTTIME ΔSST FOR FEB 15-MAR 16, 1979
ΔSST VALUES FOR EAST COAST OF AUSTRALIA

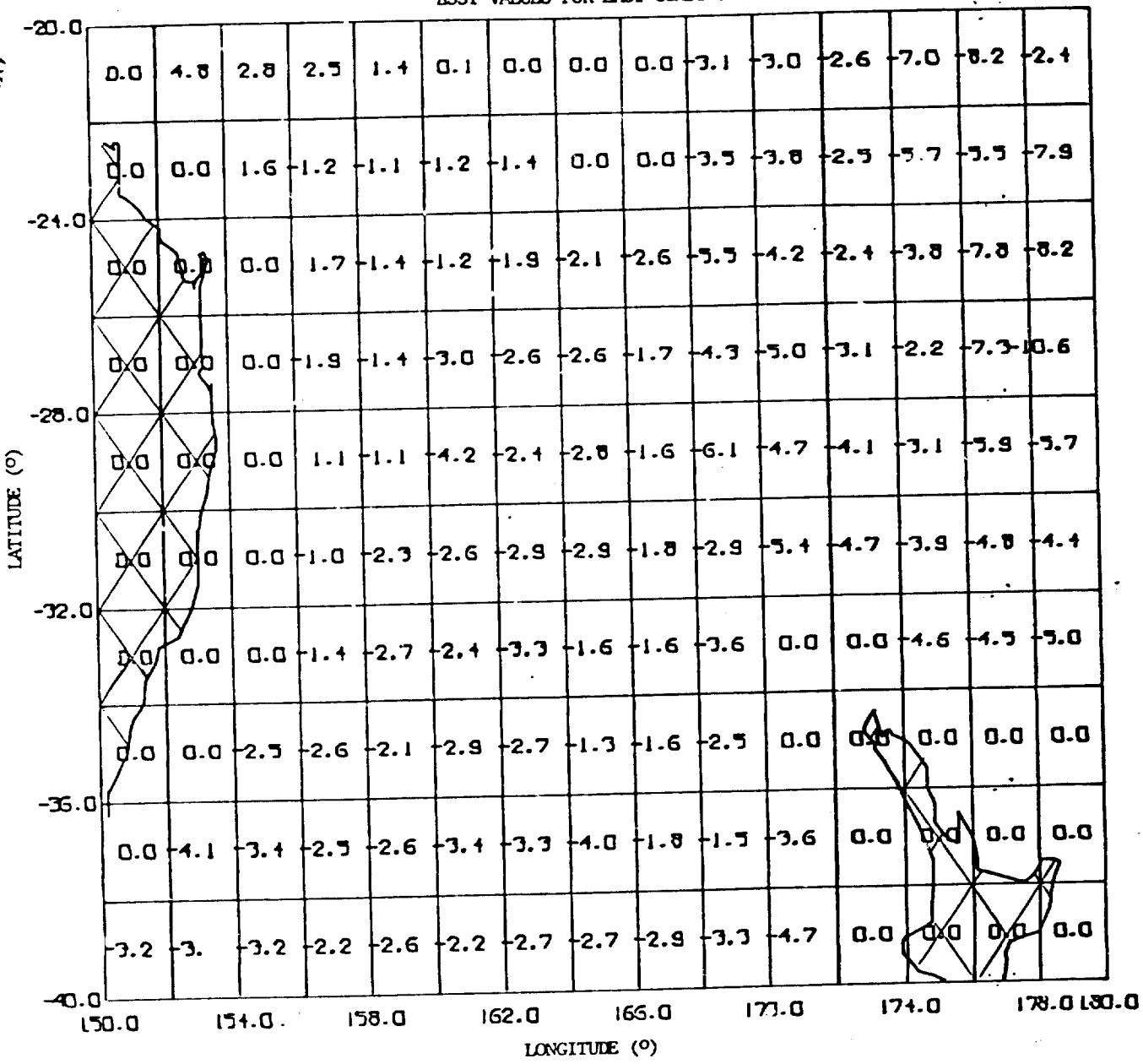

FIGURE 2.0-21. NIGHTTIME $\Delta\overline{SST}$ FOR FEB 15-MAR 16, 1979

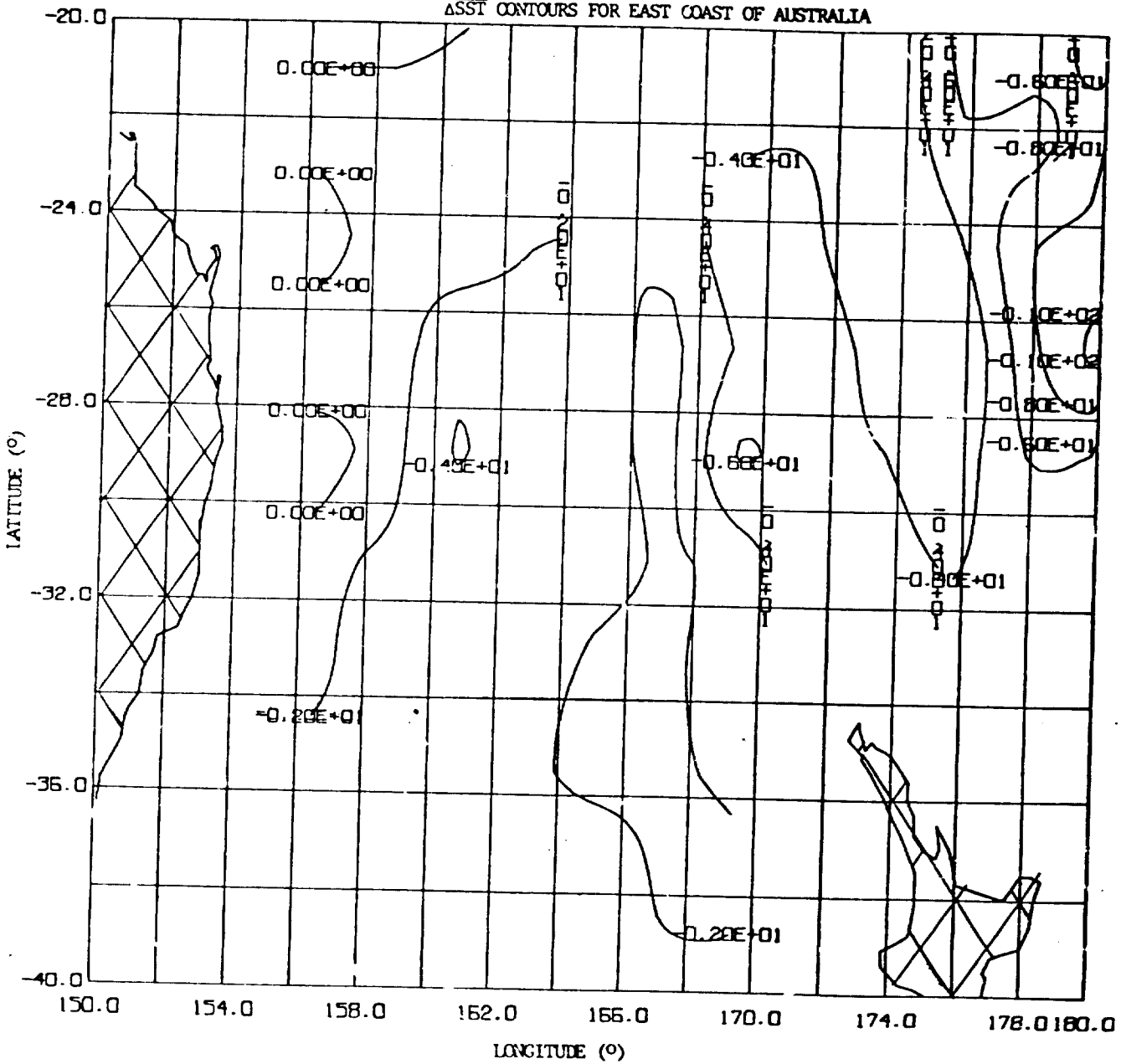

FIGURE 2.0-22. DAYTIME $\Delta\overline{SST}$ FOR FEB 15-MAR 16, 1979
$\Delta\overline{SST}$ VALUES FOR WEST COAST OF SOUTH AMERICA

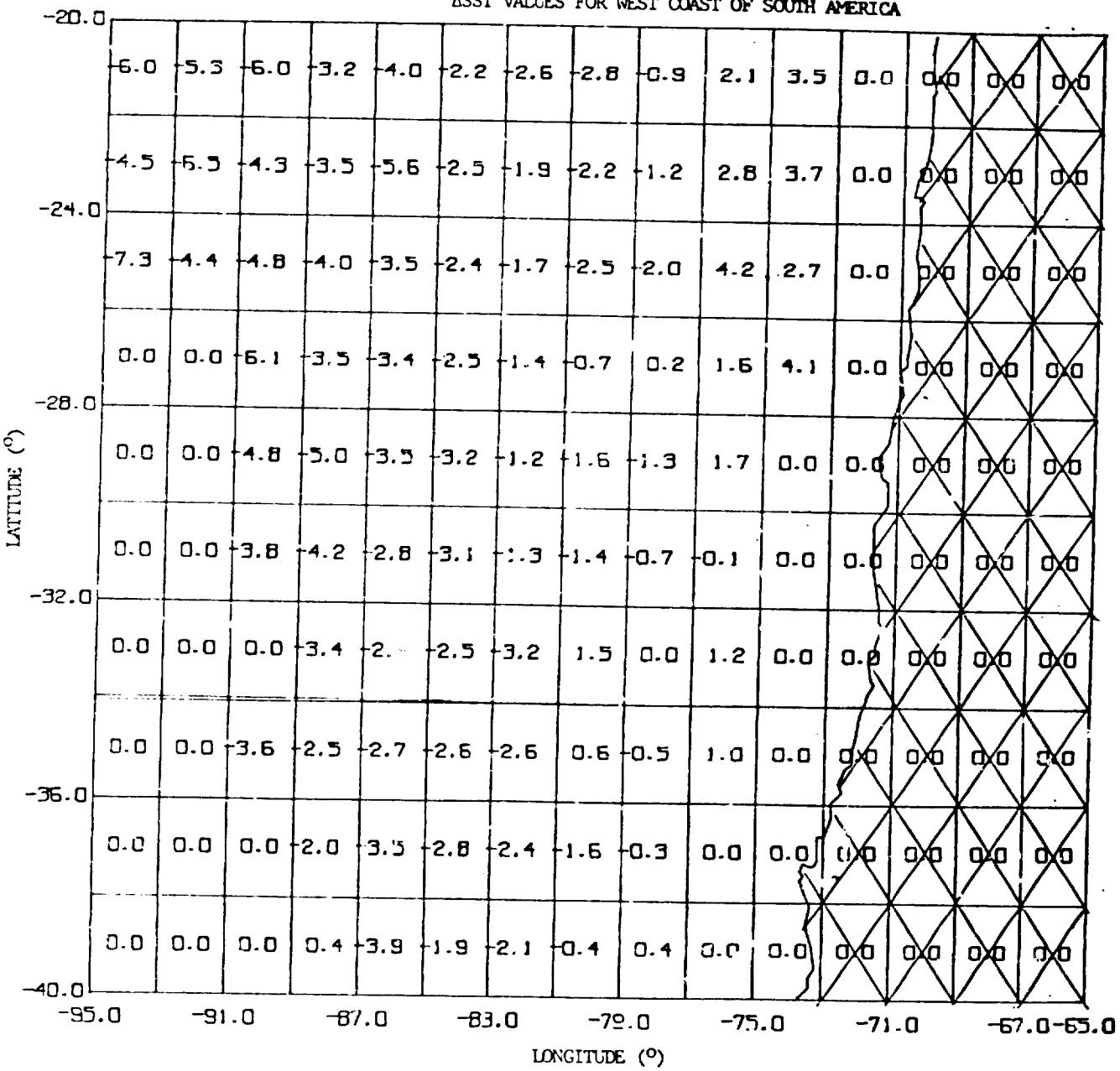

FIGURE 2.0-23. DAYTIME $\Delta\overline{SST}$ FOR FEB 15-MAR 16, 1979
$\Delta\overline{SST}$ CONTOURS FOR WEST COAST OF SOUTH AMERICA
Note lines of constant $\Delta\overline{SST}$ running parallel to the coast and decreasing nearly monotonically with distance from land.

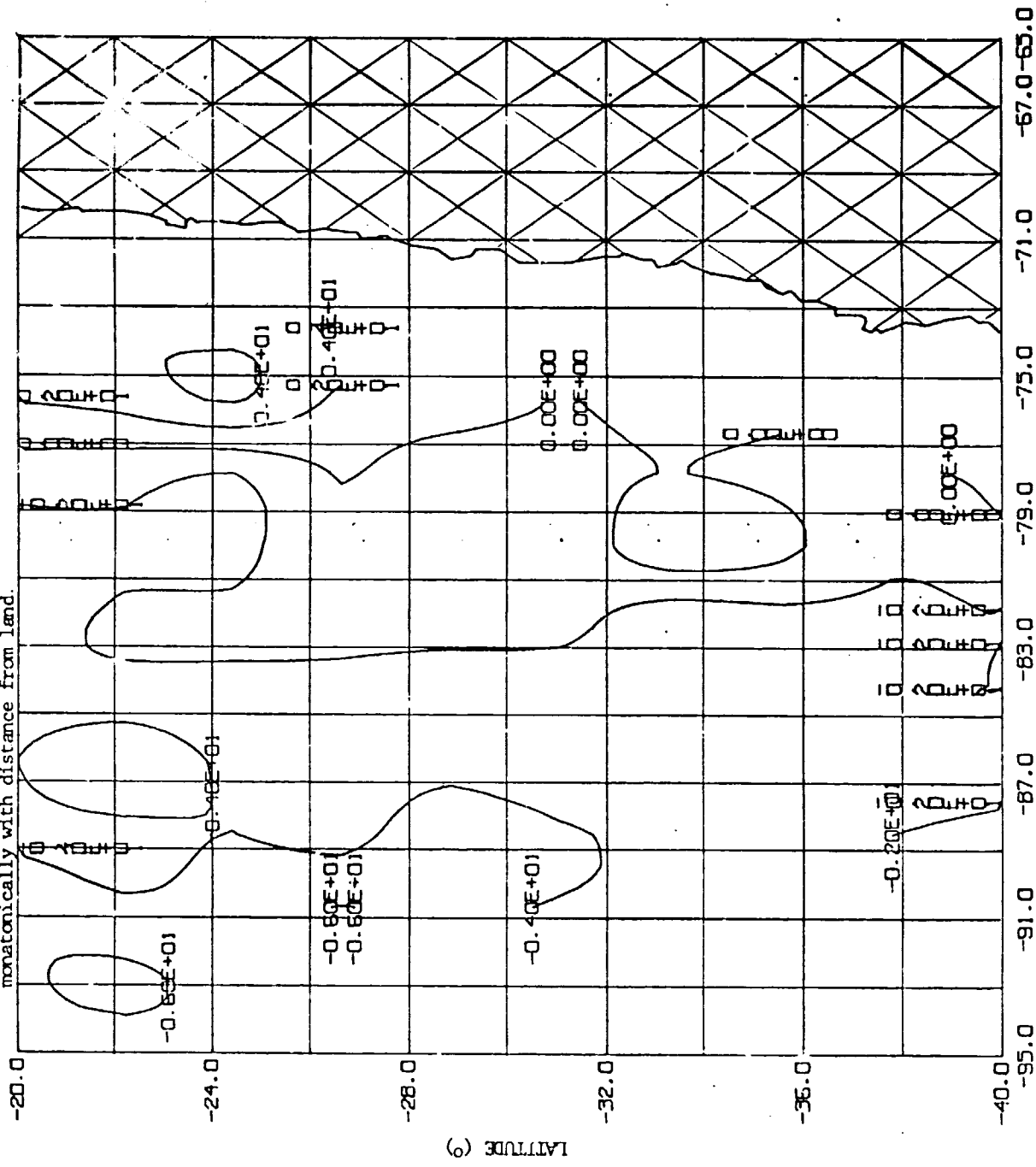

FIGURE 2.0-24. NIGHTTIME $\overline{\Delta SST}$ FOR FEB 15-MAR 16, 1979

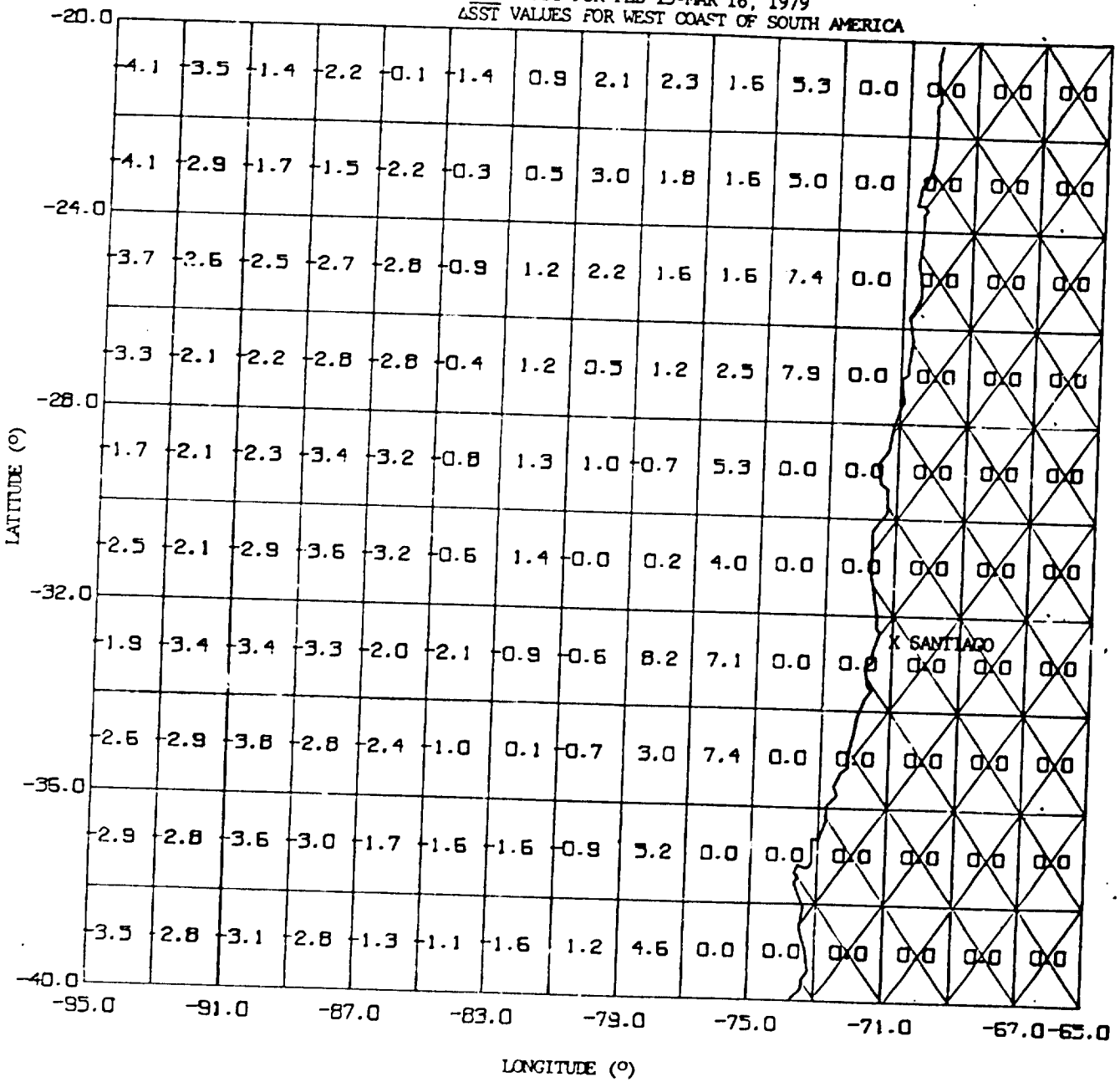

FIGURE 2.0-25. NIGHTTIME $\Delta\overline{SST}$ FOR FEB 15-MAR 16, 1979
$\Delta\overline{SST}$ CONTOURS FOR WEST COAST OF SOUTH AMERICA

Note lines of constant $\Delta\overline{SST}$ running parallel to the coast and decreasing nearly monatonically with distance from land.

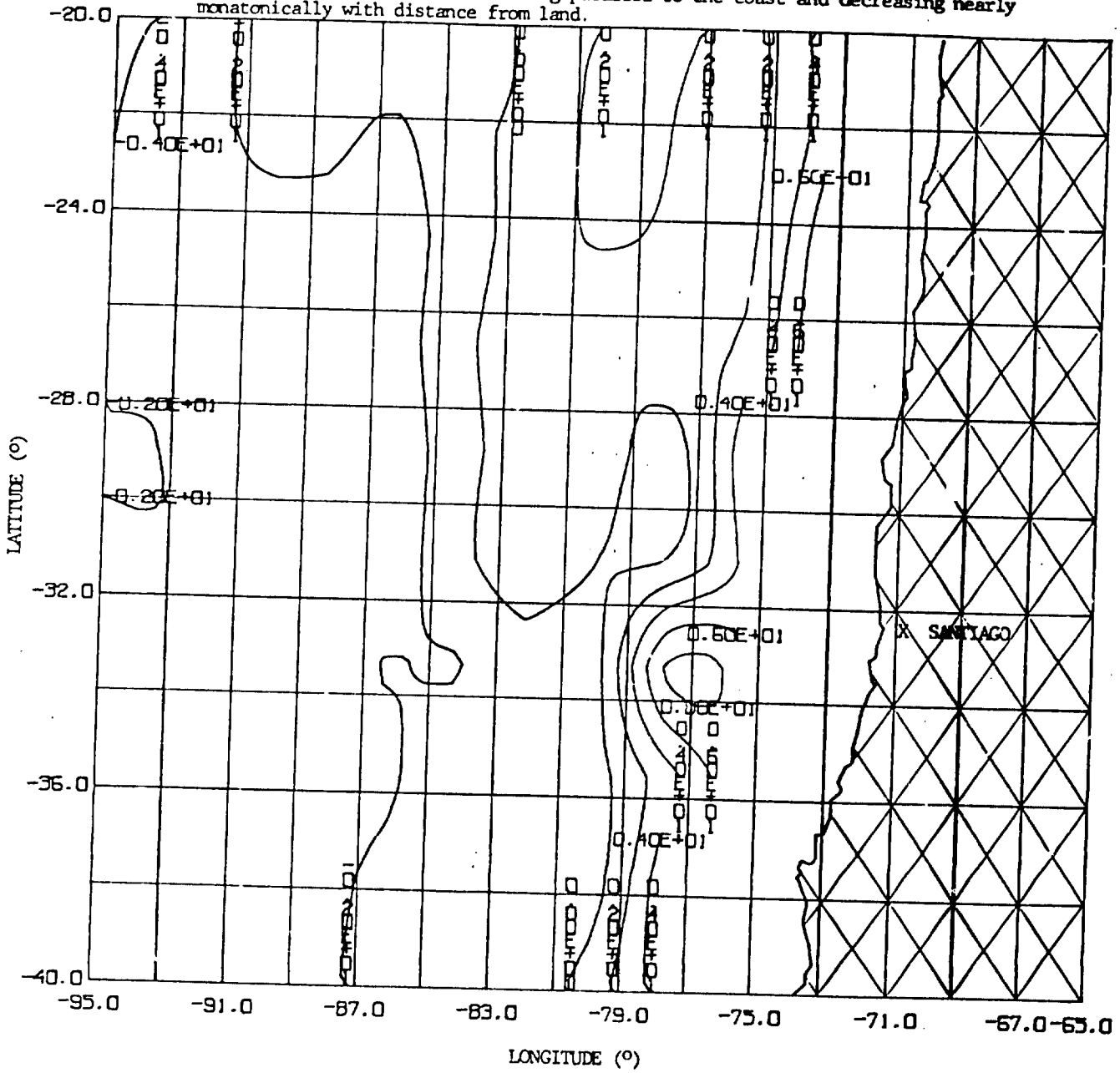

FIGURE 2.0-26. DAYTIME $\overline{\Delta SST}$ FOR FEB 15-MAR 16, 1979
$\overline{\Delta SST}$ VALUES FOR EAST COAST OF SOUTH AMERICA

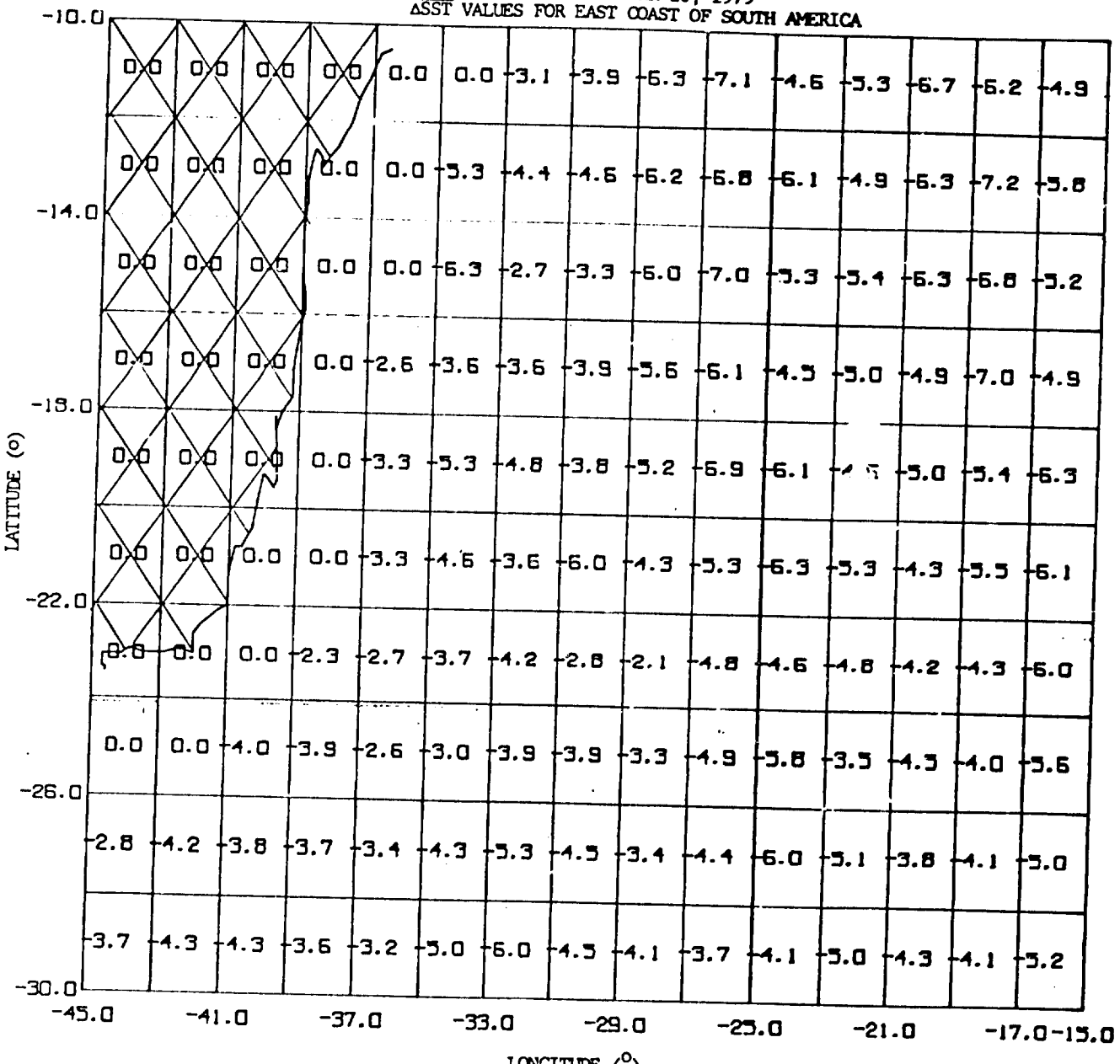

FIGURE 2.0-27. DAYTIME $\Delta\overline{SST}$ FOR FEB 15-MAR 16, 1979
$\Delta\overline{SST}$ CONTOURS FOR EAST COAST OF SOUTH AMERICA

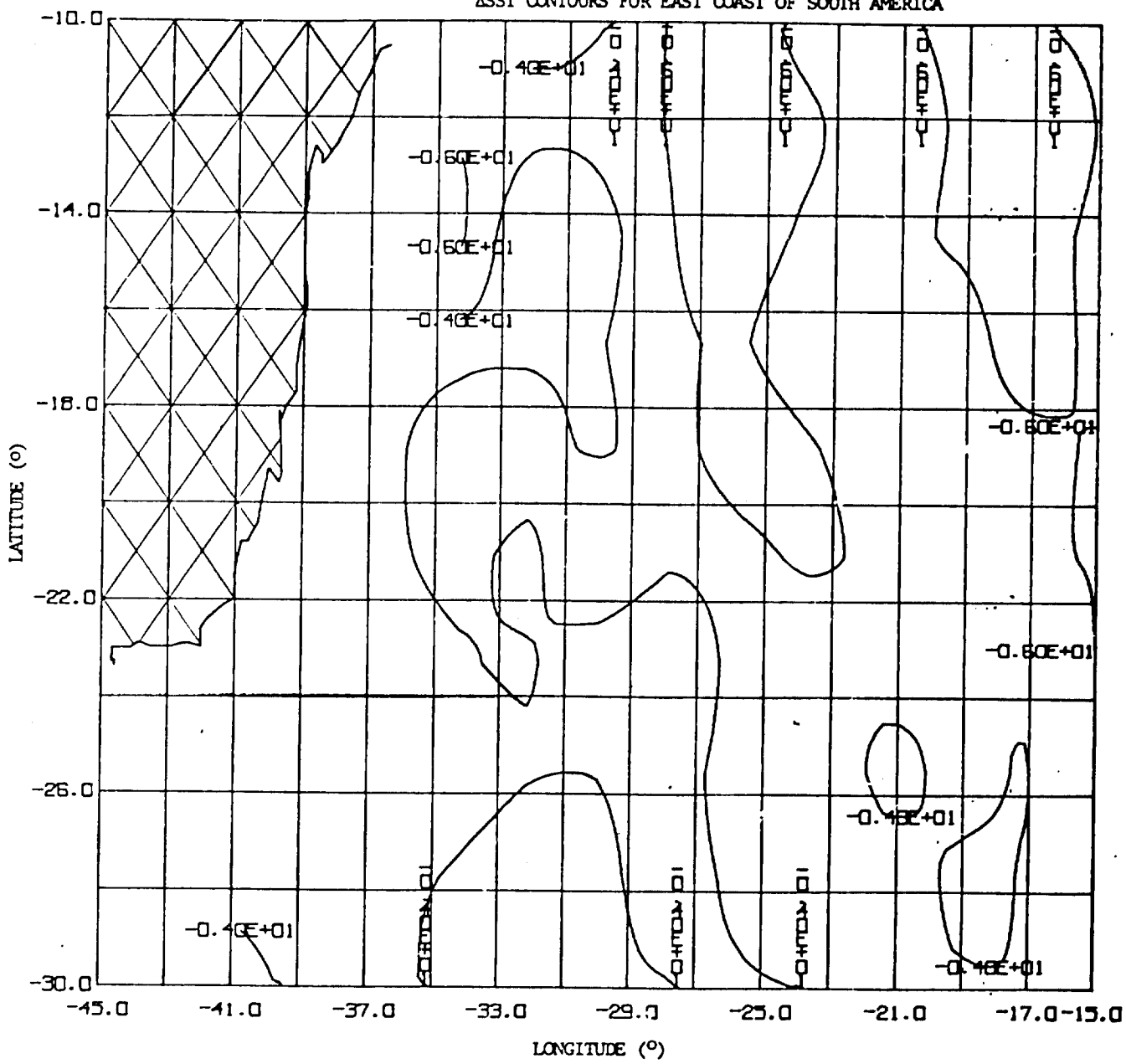

FIGURE 2.0-18. NIGHTTIME $\Delta\overline{SST}$ FOR FEB 15-MAR 16, 1979

$\Delta\overline{SST}$ VALUES FOR EAST COAST OF SOUTH AMERICA

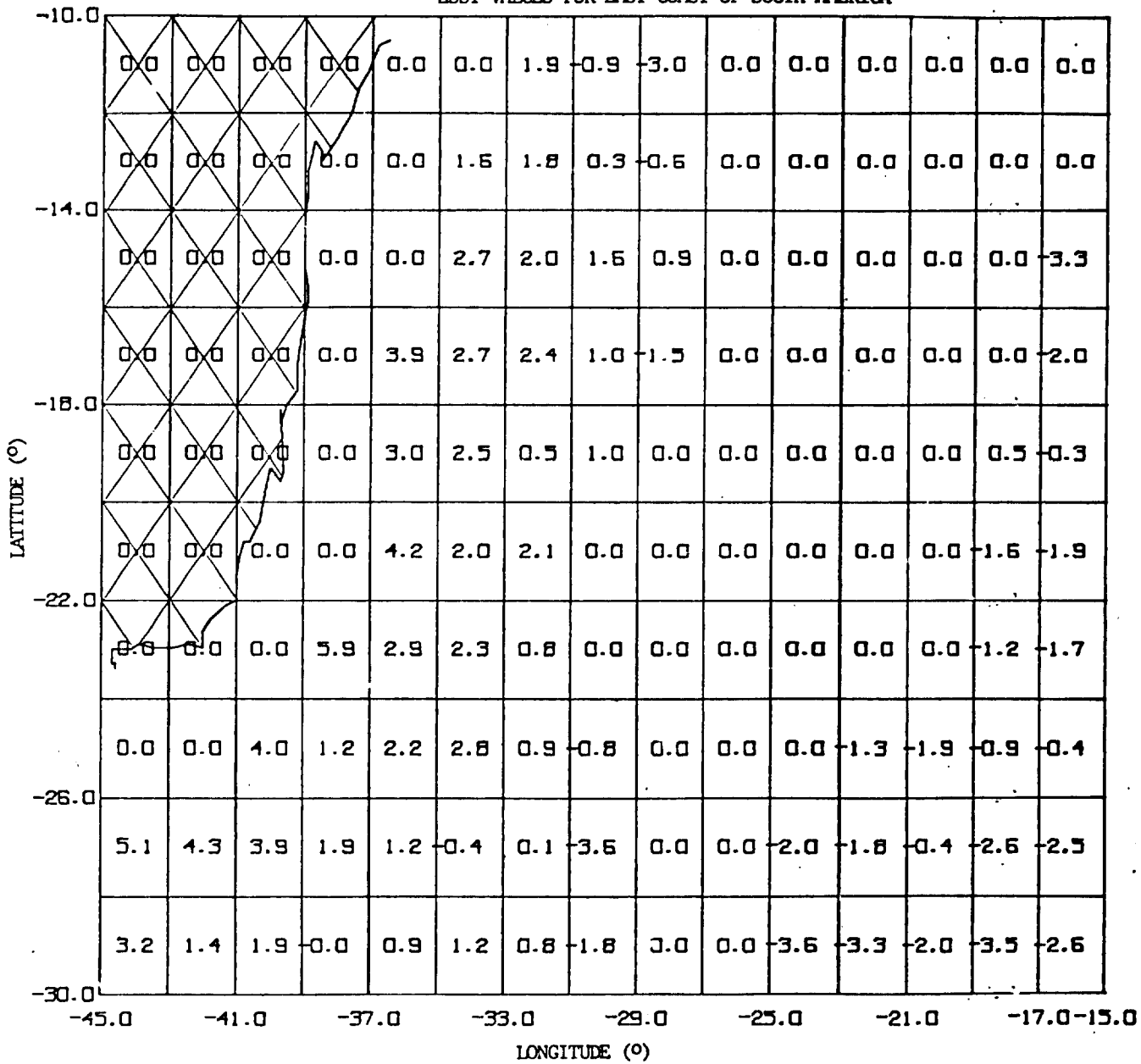

FIGURE 2.0-29. NIGHTTIME $\Delta\overline{SST}$ FOR FEB 15-MAR 16, 1979
$\Delta\overline{SST}$ CONTOURS FOR EAST COAST OF SOUTH AMERICA

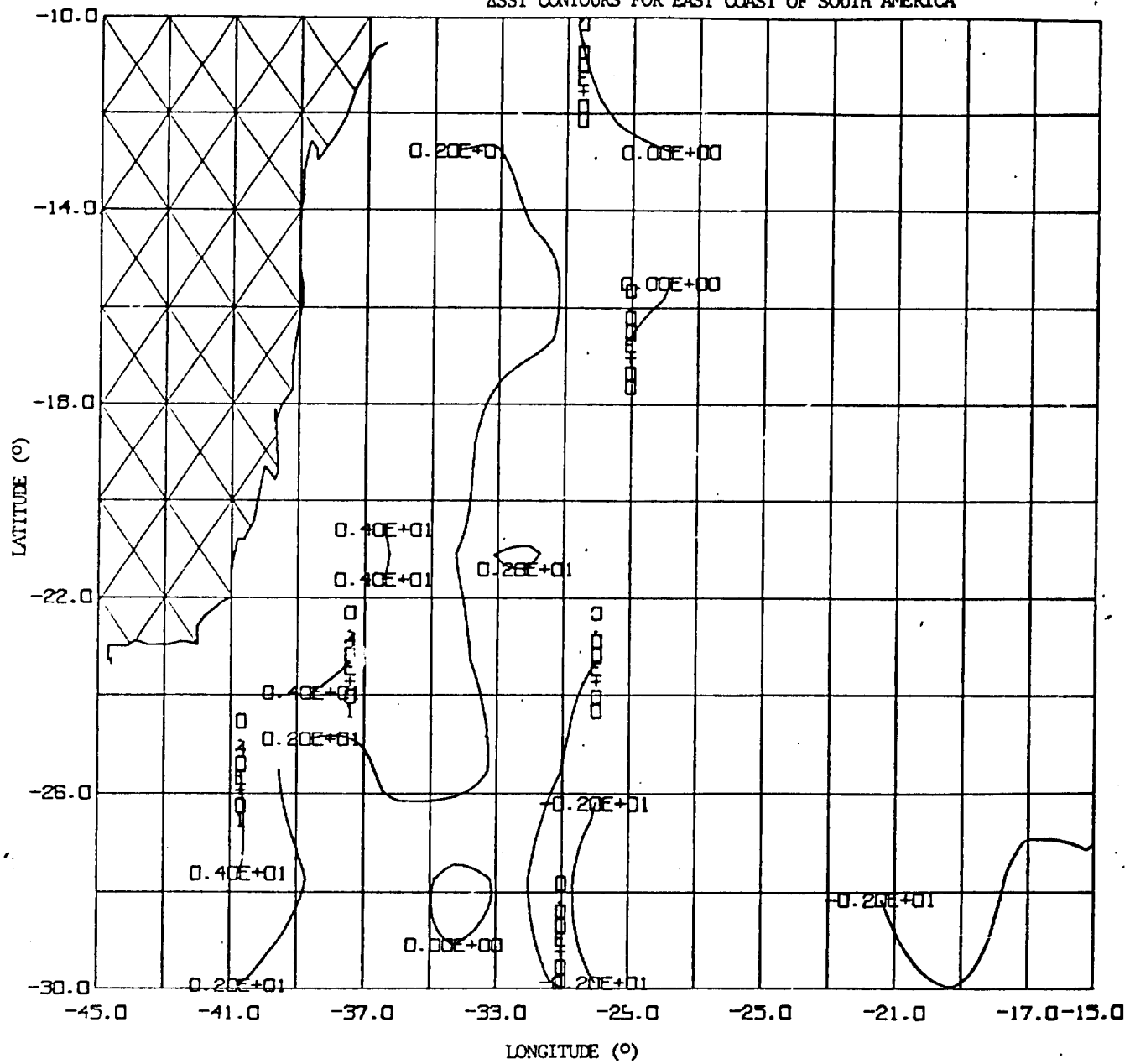

FIGURE 2.0-30. DAYTIME $\Delta\overline{SST}$ FOR FEB 15-MAR 16, 1979
$\Delta\overline{SST}$ VALUES FOR NORTHEAST COAST OF SOUTH AMERICA

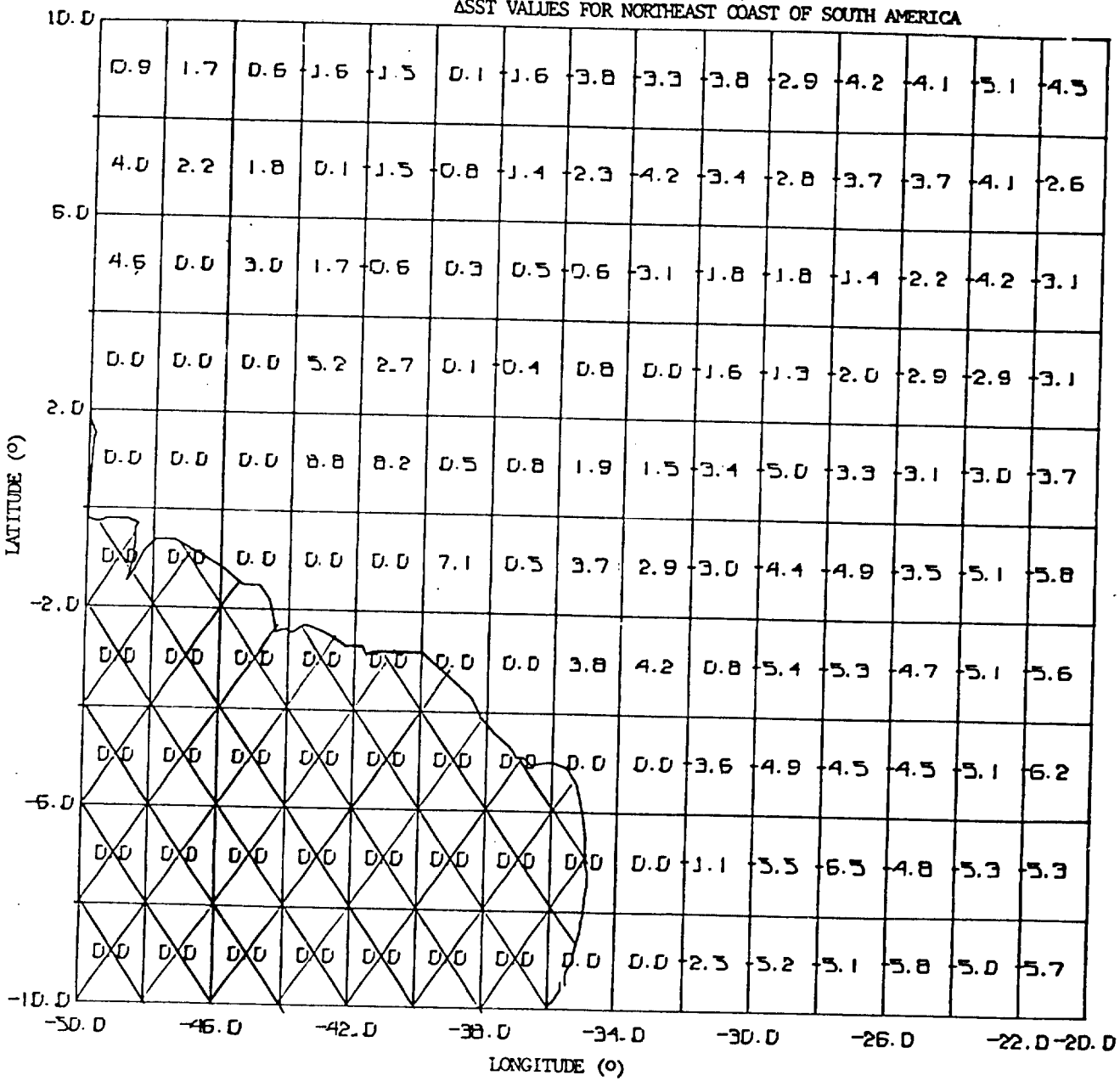

FIGURE 2.0-31. DAYTIME $\Delta\overline{SST}$ FOR FEB 15-MAR 16, 1979
$\Delta\overline{SST}$ CONTOURS FOR NORTHEAST COAST OF SOUTH AMERICA

Note lines of constant $\Delta\overline{SST}$ running parallel to the coast and decreasing nearly monatonically with distance from land.

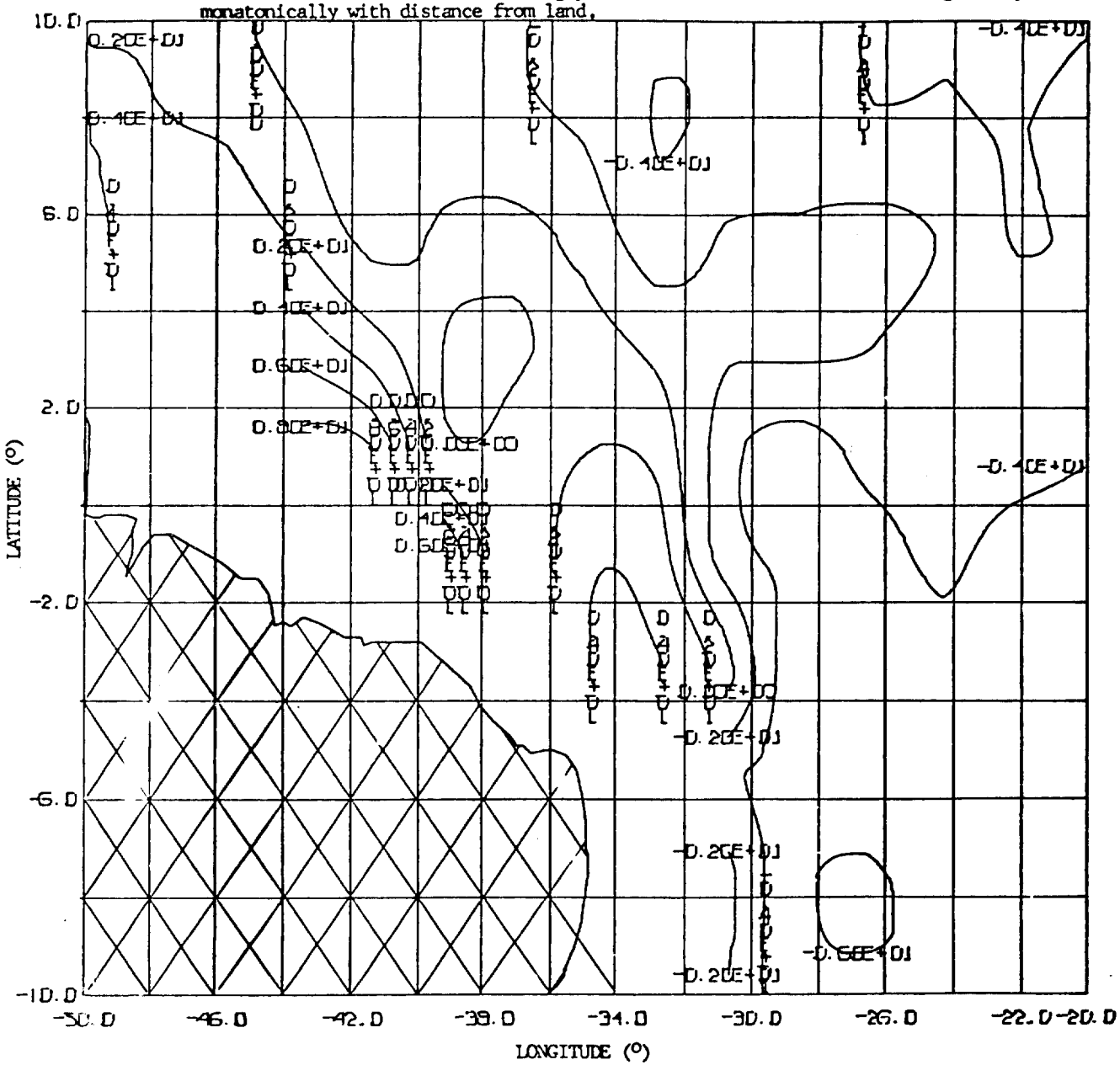

FIGURE 2.0-32. NIGHTTIME $\Delta\overline{SST}$ FOR FEB 15-MAR 16, 1979
$\Delta\overline{SST}$ VALUES FOR NORTHEAST COAST OF SOUTH AMERICA

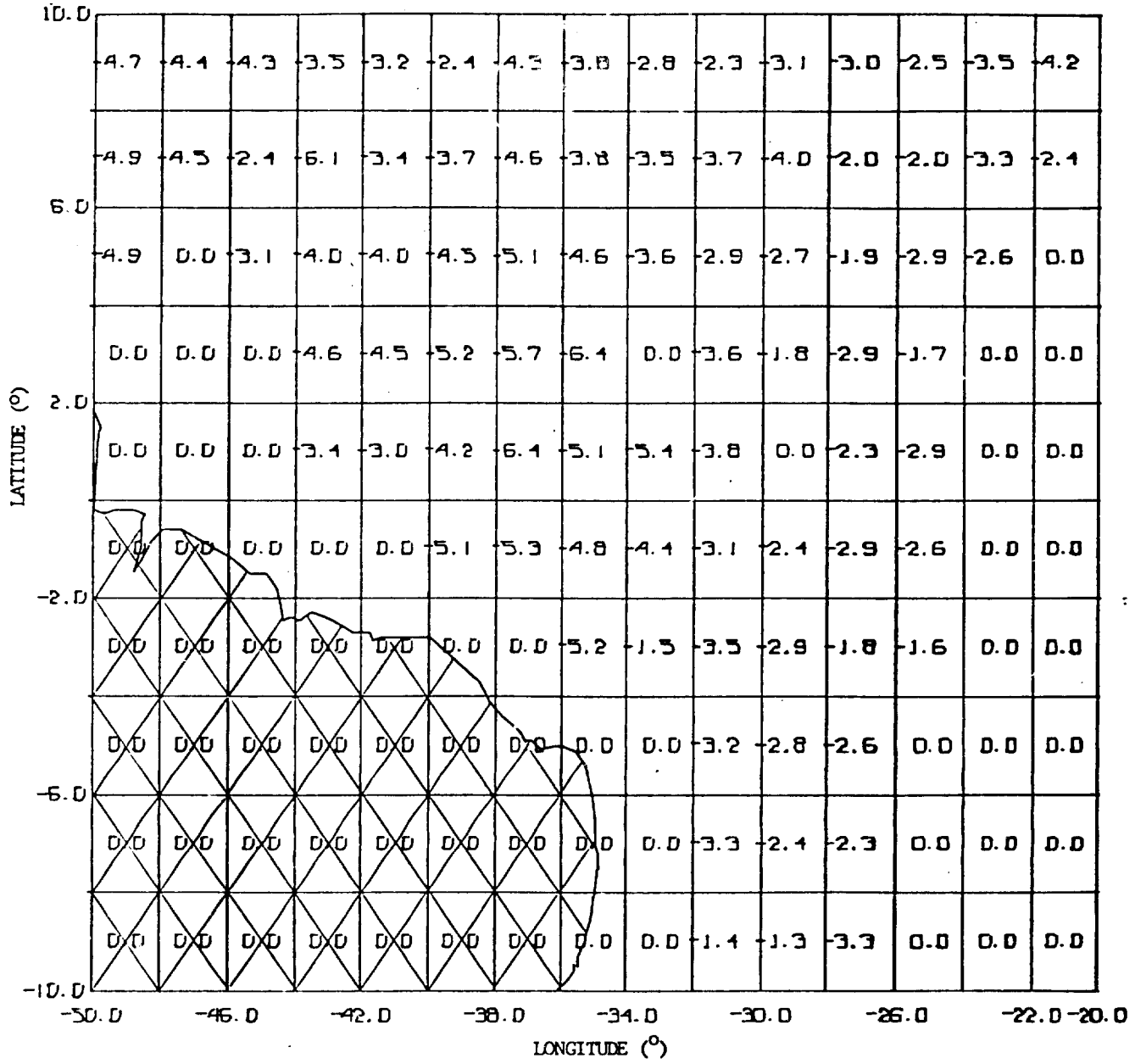

FIGURE 2.0-33. NIGHTTIME $\Delta\overline{SST}$ FOR FEB 15-MAR 16, 1979

$\Delta\overline{SST}$ CONTOURS FOR NORTHEAST COAST OF SOUTH AMERICA

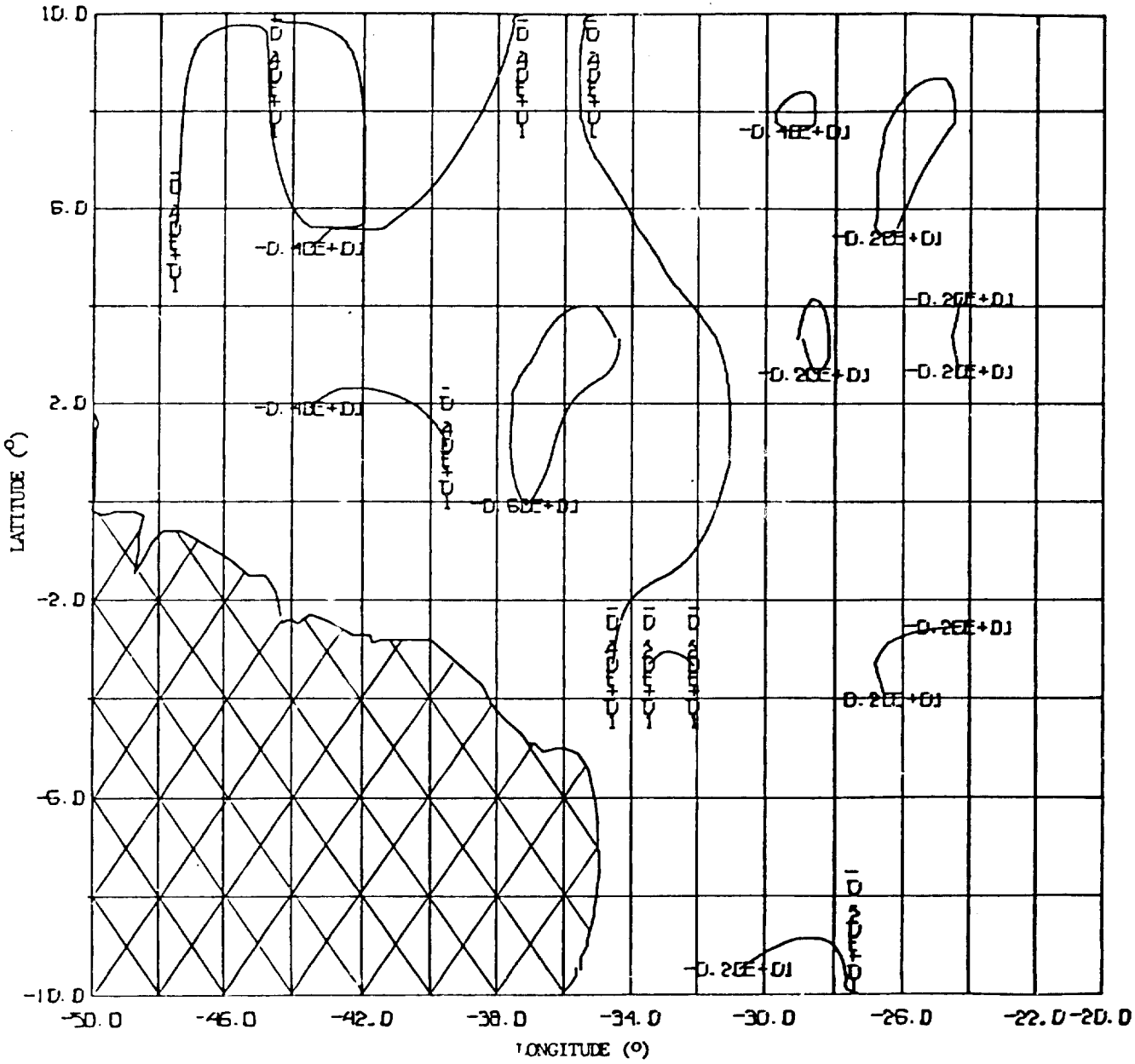

FIGURE 2.0-34. DAYTIME $\overline{\Delta SST}$ FOR FEB 15-MAR 16, 1979
$\overline{\Delta SST}$ VALUES FOR SOUTHWEST COAST OF AFRICA

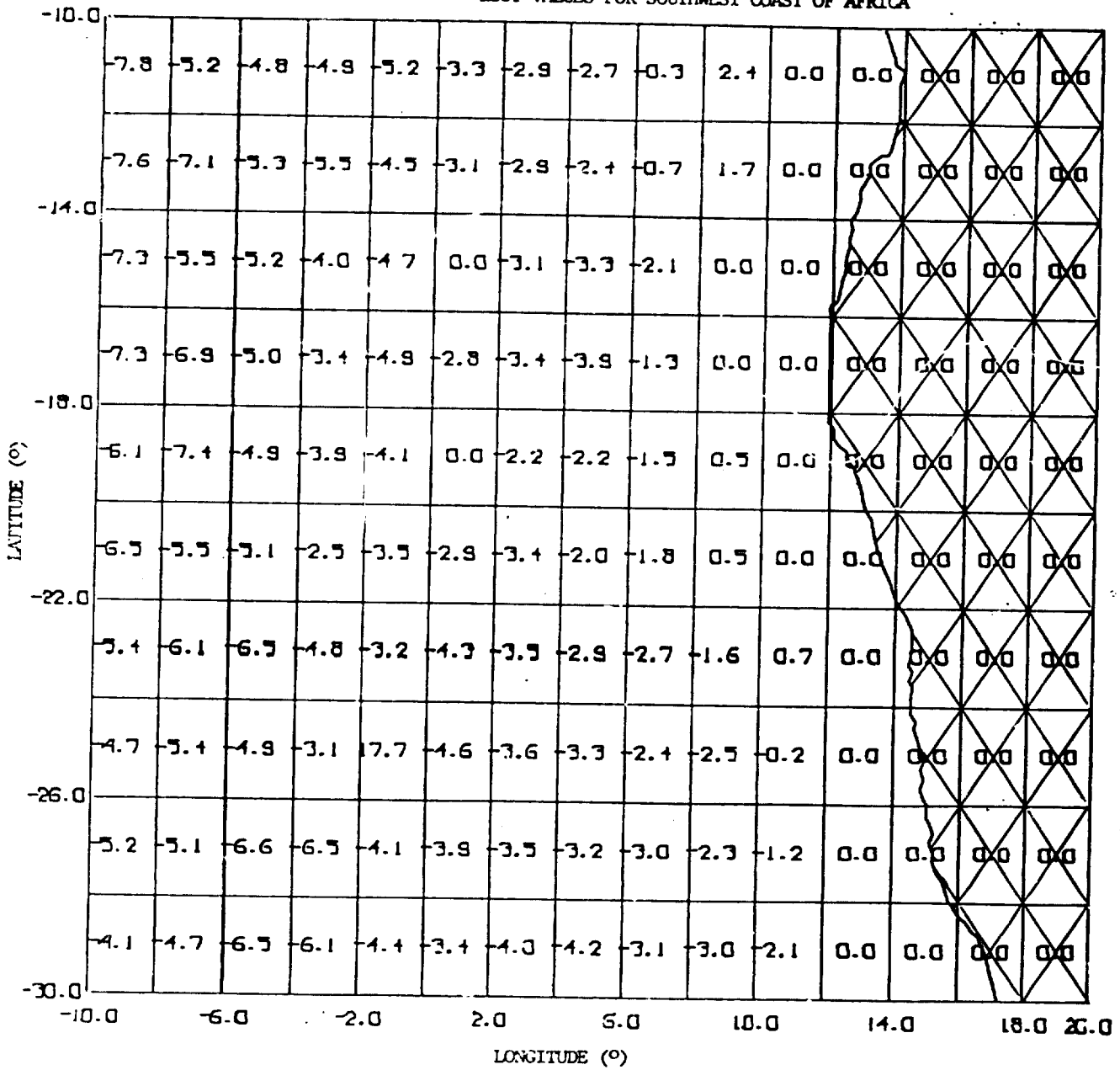

FIGURE 2.0-35. DAYTIME $\Delta\overline{SST}$ FOR FEB 15-MAR 16, 1979
$\Delta\overline{SST}$ CONTOURS FOR SOUTHWEST COAST OF AFRICA

Note presence of intense RFI occurance on Feb 23, 1979 in average.

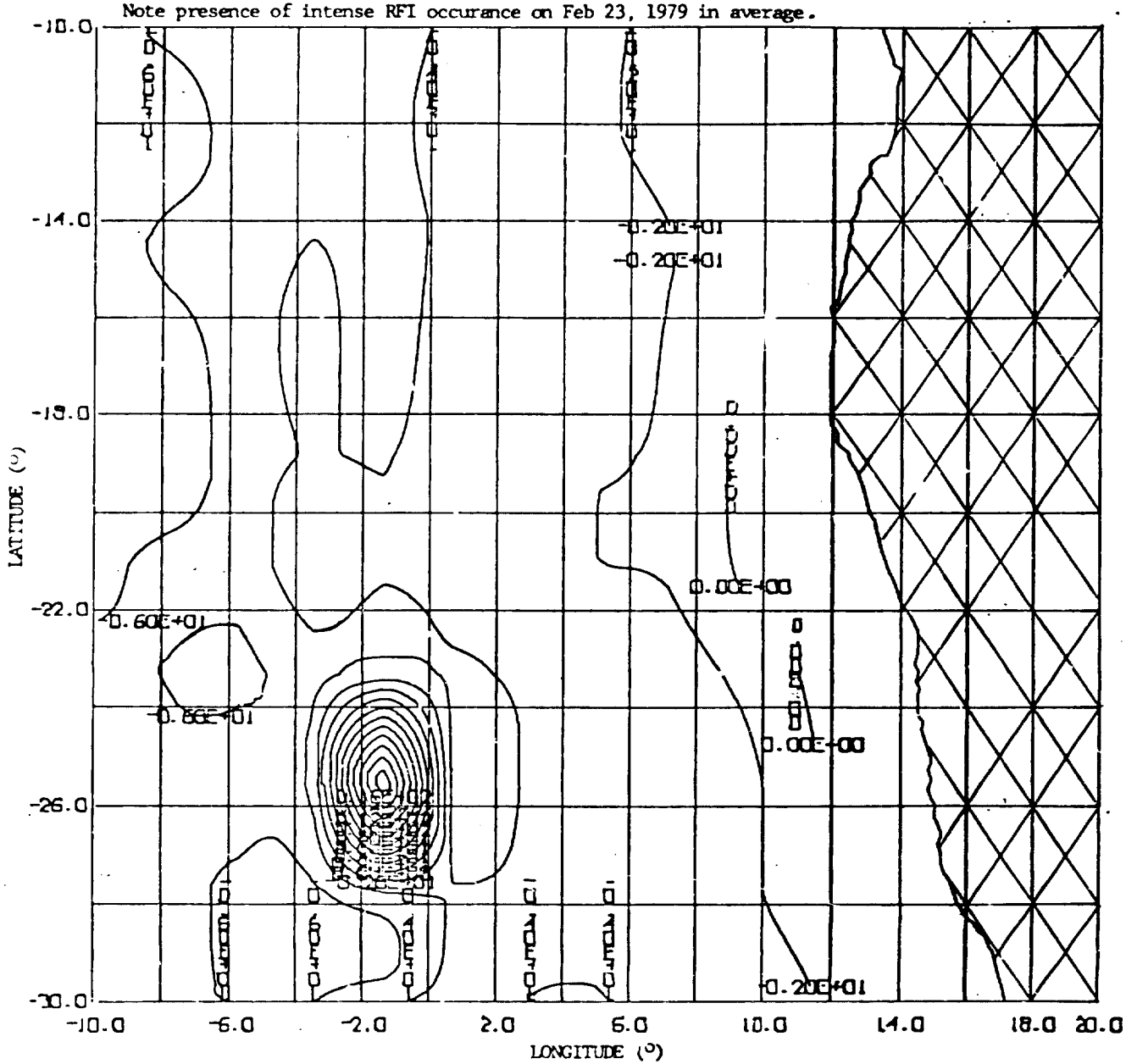

FIGURE 2.0-36. NIGHTTIME $\Delta\overline{SST}$ FOR FEB 15-MAR 16, 1979
$\Delta\overline{SST}$ VALUES FOR SOUTHWEST COAST OF AFRICA

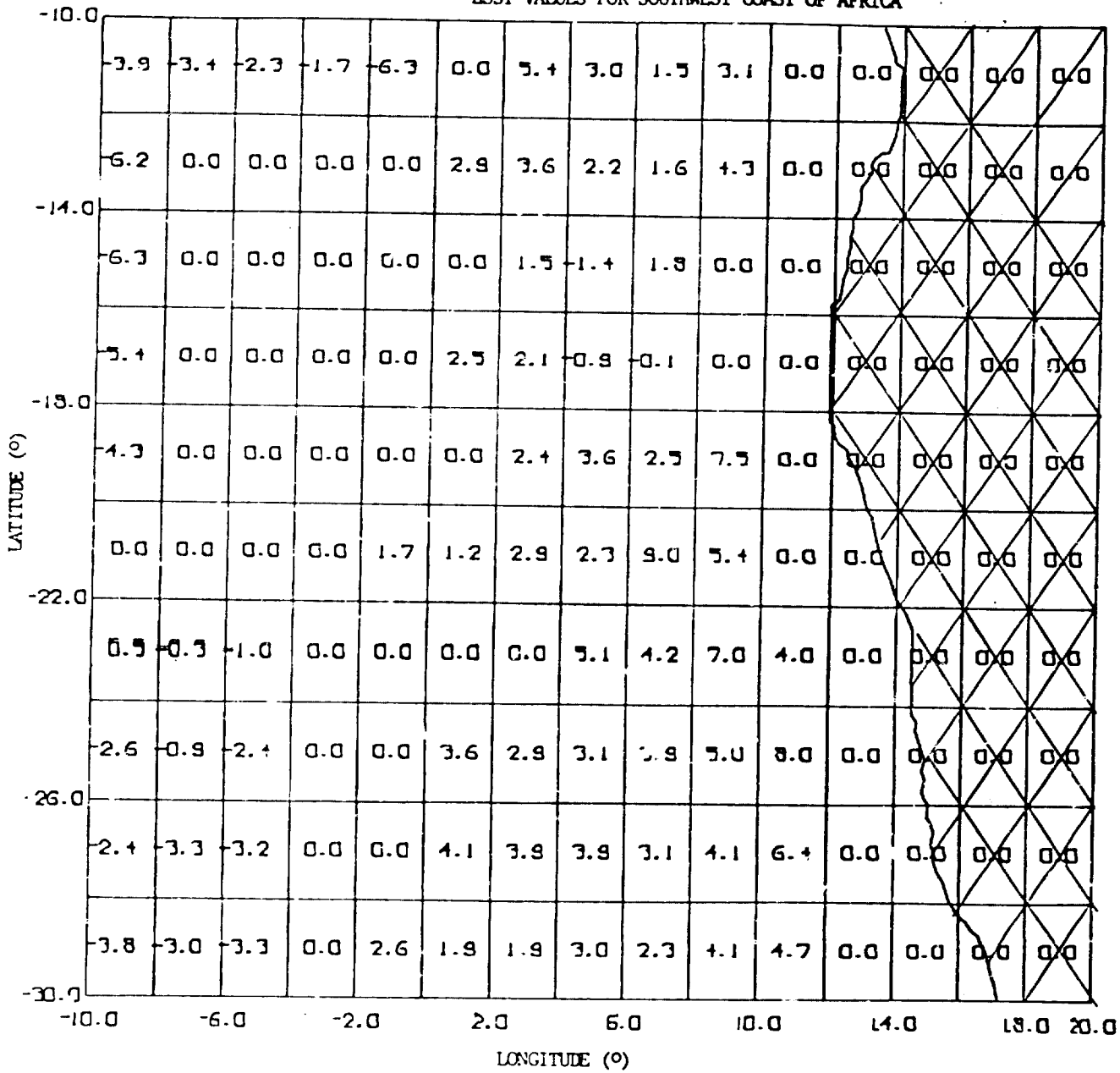

FIGURE 2.0-37. NIGHTTIME $\Delta\overline{SST}$ FOR FEB 15-MAR 16, 1979
$\Delta\overline{SST}$ CONTOURS FOR SOUTHWEST COAST OF AFRICA

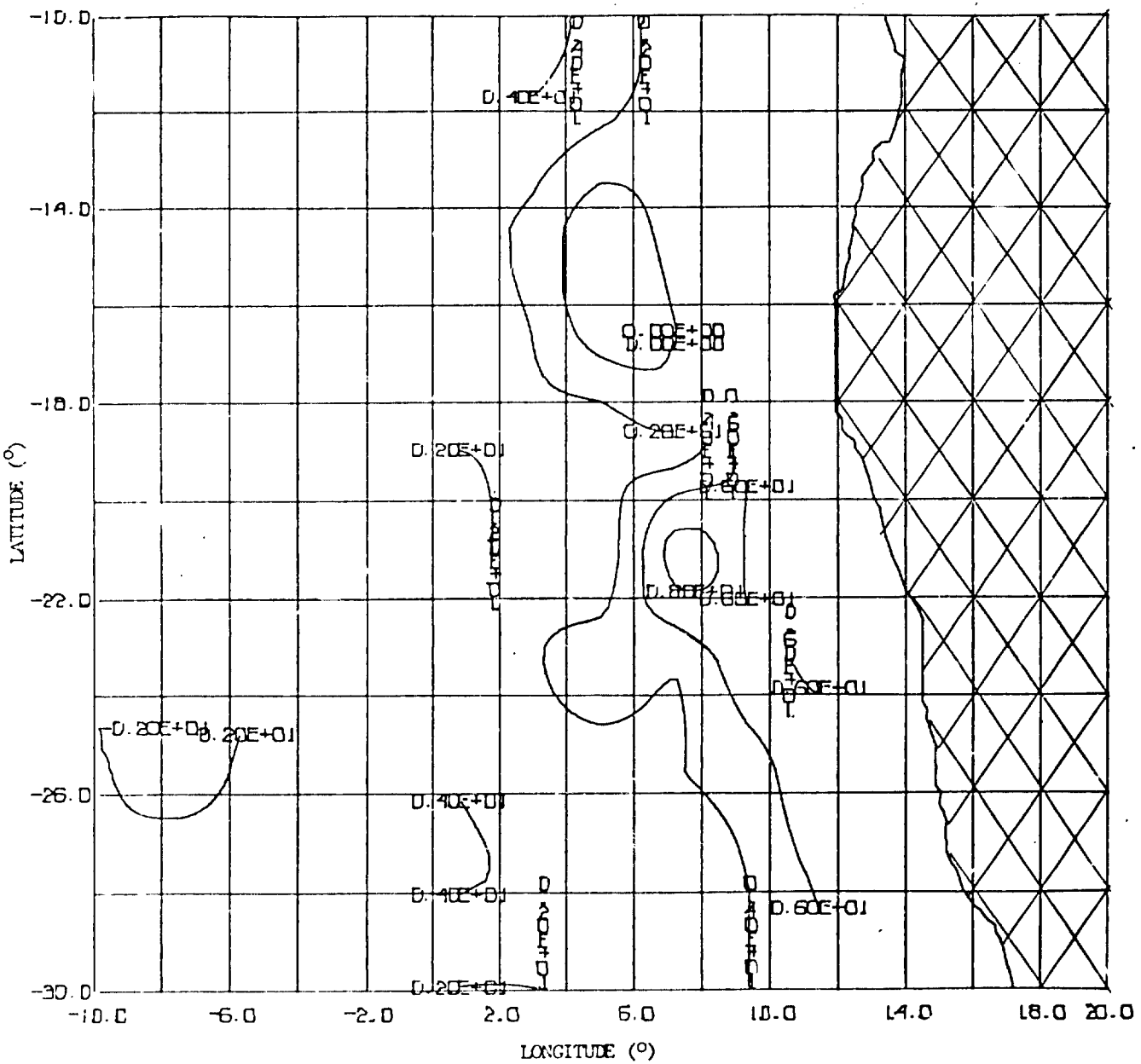

3.0 CONCLUSIONS

Based on this preliminary study of a very limited amount of SMMR data several conclusions concerning the presence of radio frequency interference in the SMMR sea surface temperature retrievals can be drawn.

Intense isolated point sources of ocean RFI can easily be identified by looking for abnormally high SST or brightness temperature values. Intense RFI has been noticed in 35 cases for the 42 days of test data, and the occurances tend to cluster in several geographical areas. The 6.6 GHz vertical channel on SMMR is affected most by these intense RFI occurances, with some effect evident in the 6.6 GHz horizontal channel, and practically none at the other SMMR frequencies.

Examination of SMMR SST data in eight coastal regions on the globe for a month, indicates radio frequency interference can be significant enough to cause unacceptable errors in SMMR SST retrievals at distances up to 1000 km from the coastline. In addition some other effect arising from the relative geometry of the coastline and the SMMR scanning pattern may be present in the SMMR data, and therefore may be superimposed on the coastal RFI signature.

The existence of RFI in the 6.6 GHz band not only distorts the SMMR SST retrieval, but also raises questions concerning frequency selection for future spacecraft. To answer these questions the SMMR data needs to be analyzed on a global basis using a more extensive set of observations. This more complete analysis can be done using the existing data base of over a year's worth of SMMR antenna temperature observations, and the expanded brightness temperature data set which will soon be available.

In addition a simulation of coastal RFI using known transmitter patterns with the SMMR antenna pattern can produce RFI signatures which can be compared with actual observations in order to separate RFI contributions from other effects present in the data.

4.0 REFERENCES

Friebaum, J. "Remote Sensing - Potential Interference Problems and Solutions", pp. 173-181, Proceeding of the International Symposium on Remote Sensing of the Environment, Volume 1, 1975.

Wilheit, T.T., and Chang, A.T.C., An Algorithm For Retrieval of Ocean Surface and Atmospheric Parameters From the Observations of the Scanning Multichannel Microwave Radiometer, Radio Science, 1980.